NUMERICAL AND ANALYTICAL ANALYSES OF HIGH-STRENGTH STEEL CELLULAR BEAMS: A DISCERNING APPROACH.

Rabee Shamass [a], Federico Guarracino [b]

[a] *Division of Civil and Building Services Engineering, School of Build Environment and Architecture, London South Bank University, UK*

[b] *Department of Structural Engineering University of Naples `Federico II', Via Claudio 21 80125 Napoli, Italy*

Abstract

The behaviour of cellular beams made from normal and high strength steel with various geometries is investigated through a large number of finite element analyses and a simple mechanical model for the Web-Post Buckling (WPB) failure is developed and analysed in order to highlight the factors which influence its occurrence and development for both normal and High-Strength (HS) steels. The performed FE analyses and the proposed modelling, once calibrated, allow to shed some light on the characteristics of the phenomenon and to provide the basis of a reliable design method to predict shear buckling of web-post of cellular beams made both of mild and HS steel.

Keywords: Cellular beams; Web-Post Buckling; High Strength steel.

1. Introduction

Cellular steel beams are widely used in modern constructions due to their economic and aesthetic advantages, compared to solid I-beam. They are applicable to situations where services (e.g. conduits for ventilation or air conditioning) are to be fitted within required structural depths or long spans are requested along with desirable creative appearance. They are manufactured from hot-rolled I-beam section by cutting along web length in a certain pattern to create the upper and lower halves of the cellular beam and re-welding again to form a cellular beam, as seen in the Figure 1, where H is the total height of the cellular section; t_w is the web thickness; t_f is the flange thickness; b_f is the flange width; d is the height of the parent section; d_o is the opening diameter; s is the centre-to-centre spacing of adjacent openings; s_o is the edge-to-edge spacing of adjacent opening. The opening up of rolled beam increases its section modulus and moment of inertia, resulting in greater strength and rigidity. The reduction in the beams weight has an obvious effect on material and handling cost.

Unfortunately, the flexural behaviour of cellular I-shaped steel beam can be a complex issue on account of its susceptibility to several failure types and instability modes: Vierendeel bending (VB) due to shear distribution across the opening (Figure 2a), overall bending failure (BF) (Figure 2b), shear failure (SF) due to reduced steel section (Figure 2c), web-post

buckling (WPB) due to horizontal shear force in the web-post (Figure 2d), lateral torsional buckling (LTB) (Figure 2e), and rupture of weld joints (Figure 2f).

Many experimental tests have been conducted on cellular beams with different geometries to investigate their structural behaviour and failure modes. Tsavdaridis and D'Mello [4] tested closely spaced web openings of various shapes and found that all the tested cellular beams failed by WPB. More recently Grilo et al. [5] tested nine cellular beams and the WPB failure dominates the failure of all beams. Erdal and Saka [6] tested 12 cellular beams and found that 6 beams failed by WPB and two beams failed by combined WPB and VB. Panedpojaman et al. [7] tested 9 cellular beams with different geometries and loading conditions (i.e. one or two point loads) and found that seven beams failed by WPB and two beam failed by combined WPB and LTB. It can be noted from the various experiments that web-post buckling is typically the limiting cause, especially for large closely spaced openings ones.
An early empirical design method approaching the WPB failure was officially published by SCI publication 100 [1] and was adopted by AISC [8] for the design of castellated and cellular beams. The design curves of the web-post were obtained from a series of validated non-linear finite element analyses of single web-post model. Another empirical web-post buckling model proposed by Tsavdaridis and D'Mello [4] was derived from the finite element analyses and depends on the opening-spacing ratio and opening-web thickness ratio. Lawson et al. [9] proposed a different design methodology to calculate the shear buckling resistance based on the design strut analogy in which an effective length in the compressed diagonal strut is determined, and the compression stress resistance in this diagonal strut is calculated using the BS 5950-1:2000 compression resistance formulation or the relevant buckling curve of Eurocode 3 [10]. Panedpojaman et al. [7] proposed further improvement of the effective length of the strut model that takes into consideration the effect of the strut's boundary conditions. Grilo et al. [5] proposed a new formulation to determine the shear resistance in cellular beams for the web-post buckling based on resistance curved derived from the finite element analyses.

High strength (HS) steels whose nominal yield strength exceeds 460 MPa are produced widely nowadays and there has been a strong demand worldwide for their use in many buildings and bridges structures. The use of HS steel instead of normal strength steel in steel construction can reduce the member size, leading to smaller foundations and can reduce the amount of coating material as well as lower construction and transportation costs.
HS steel has been the subject of intensive research from the structural engineering community in order to provide useful and efficient design data. The structural behaviour, failure modes and ductility of steel members made from HS steel can be significantly different from those made from conventional mild steel. The vast majority of research into HS steel has been focused on bare beam steel sections (e.g. [11-13]), column steel sections (e.g. [14-16]) and connections (e.g. [17-18]). A number of research studies has been conducted on the use of HS steel in composite structures such as composite beams (e.g [19-21]), and composite columns (e.g. [22]).

However, there seems to have been little or no research, at least in the public domain, into the web-post buckling of cellular beams made from HS steel. Current design methods proposed in the literatures to calculate the shear strength of web-post are applicable to normal strength steel Grade S235 or S355. Hence the effect of steel strength on the WPB of cellular beams is addressed in this study.

The objective of the present study is to investigate, through finite element analyses, the comparative behaviour of cellular beams made from normal and high strength steel with various geometries. Also, since there is no unanimous consensus about the design procedure for the shear resistance determination and the results obtained by various authors present significant differences when compared with each other, a simple mechanical model for the WPB failure is developed and analysed on the basis of geometrical and mechanical parameters only in order to highlight the factors which influence the occurrence and the development of the WPB both in normal and HS steels. The procedure is essentially based on the modelling proposed by Lawson et al. [9] but, differently from other methods, does not make reference to code prescriptions and focuses on the mechanics of the phenomenon only. It is shown that the proposed procedure, once calibrated with the aid of the performed FE analyses, can be used as a reliable design method to predict shear buckling of web-post of cellular beams made both of mild and HS steel and sheds some light on the characteristics of the phenomenon. It is finally worth noticing that the finite element models have been developed using commercial software ABAQUS and validated against existing experimental results conducted by Grilo et al. [5] and Tsavdaridis and D'Mello [4]. In fact, there are no tests available in the literature on the flexural behaviour of cellular beams made from HS steel and make resort to numerical models is currently the only possibility to conduct parametric studies of cellular beams geometries and their material properties. The present work aims therefore to constitute a first step towards the understanding of the buckling behaviour of cellular beams made of HS steel.

2. Development of the numerical modelling

Single web models are widely used in the literature to study the web-post buckling of cellular beam (e.g. [4,7]). However, the single web model cannot capture the structural behaviour of cellular beams such as deflections along the span and post-buckling behaviour. Furthermore, there is no consensus about the ideal boundary condition for these models. Therefore, here a full beam model has been developed using finite element software ABAQUS. The numerical model of the beams is validated against the specimens tested by Tsavdaridis and D'Mello [4] and Grilo et al. [5].

The elastic-plastic material model uses Von Mises yield criterion with associated plastic flow and isotropic hardening. The uniaxial behaviour of steel is modelled using multi-linear stress-strain relation, as shown in Figure 3. This relation is defined using Young modulus $E = 210$ Gpa, yield stress f_y, yield strain $\varepsilon_y = \frac{f_y}{E}$, strain at the onset of hardening ε_{st}=1.8%, ultimate stress f_u, and corresponding ultimate strain $\varepsilon_u = 15\%$. The values of f_y and f_u can be

obtained according to Grilo et al. [5] for specimens A1, A2, A3, A5, A6, B1, B2, B5 and B6, and Tsavdaridis and D'Mello [4] for specimen C1 and C2. The "engineering" stresses and strains are converted into "true" stresses and strains in the numerical model in order to consider the effects of the reduction of the cross-section during the tensile test. The formulae for conversion are:

$$\sigma^{\text{true}} = \sigma(1 + \varepsilon)$$

$$\varepsilon^{\text{true}} = \ln(1 + \varepsilon)$$

The cellular steel beam section and stiffeners are modelled using a general-purpose three-dimensional reduced integration shell element, named S4R. This element is widely used for industrial applications since it provides robust and accurate solutions in all loading conditions for thin and thick shell problems and is suitable for large-strain analysis. The size of the mesh element plays an important role in the accuracy of the results and thus a mesh sensitivity analysis has been performed for various element size. It was found that that a balanced mesh density providing both a good accuracy of the FE results and a reasonable computational cost corresponded to an element size of 15 mm for all studied cellular beams.

The boundary conditions of the cellular beams are simply supported at the bottom edges and the loading is applied under displacement-control on the top flange in the downward direction (Figure 4).

Grilo et al. [5] stated that the vertical point load was applied with an eccentricity of 20 mm of the mid-span in order to induce the web-post buckling, while Tsavdaridis and D'Mello [4] applied the loading at the mid-span of the beams C1 and C2.

Tie contact was defined between the surface of steel section and the edges of the stiffeners. A point at the mid-span of the beams was laterally restrained in order to prevent the specimens from buckling in a lateral torsional mode. Two analyses have been conducted: first a linear buckling analysis in order to obtain eigenvalues and eigenmodes and, successively, a nonlinear analysis using a Newton-Raphson solution method in order to obtain the buckling load and to follow the post-buckling path of the beam after failure. Geometrical imperfections due to the process of cutting and fabrication of the cellular beams are inevitable and can cause significant drops of the value of the buckling load. The imperfections contribute to initiate the bucking and their post-buckling behaviour is affected by the size and shape of the geometrical imperfections. Thus, in order to obtain reliable and accurate numerical results, initial imperfections were included in the FE model. The initial imperfection shape used in the numerical analysis has been based on the lowest buckling mode obtained from the linear buckling analysis in order to apply the most critical imperfection. The imperfection amplitude was assumed to be equal to $\delta_w/25$ for the specimens tested by Grilo et al. [5] (δ_w is the imperfection measured value) as it led to the most accurate results when the models were compared to experimental results. For the specimens C1 and C2, the imperfection size was assumed as $t_w/200=7.6/200=0.038$ mm [4].

3. Validation of the finite element model

In order to evaluate the accuracy of the beam model described above for analysing the structural behaviour of cellular beams, the buckling load, the load-deflection relationship and the failure modes for the cellular beams are compared with the corresponding experimental results obtained by Grilo et al. [5] for specimens A1, A2, A3, A5, A6, B1, B2, B5 and B6, and by Tsavdaridis and D'Mello [4] for specimen C1 and C2. Due to the symmetry of the beam model, the vertical bucking shear load of cellular beam corresponds to half of the ultimate load.

3.1 The web-post bucking resistance of the cellular beams

The numerical buckling loads for all studied specimens are presented together with their experimental counterparts in Table 1. It can be observed that the predicted loads are in very good agreement with the corresponding experimental results in which the numerical vertical shear loads differ from the experimental ones from -7.2% to 5.3% with an average deviation of -1.5%. Consequently, it can be concluded that the FE model adopted in the present study is adequate for predicting the buckling shear strength of cellular beams with various geometries.

3.2 Load-displacement response

Figure 5 shows the load vs mid-span displacement response in the numerical simulation and in the experimental setting. For brevity, only cases A2, A5, A6, B1, B2 and B6 are presented as they are reflective of the results for all specimens. It is observed that the initial bending stiffness obtained from FE model are in good agreement with those obtained experimentally for all specimens, except for A5 and A6 at which the slope of the load-displacement curves before the ultimate load is attained are higher than those observed experimentally. This can be attributed to the difference between the multi-linear stress-strain relationships of Figure 3 and the actual constitutive laws, see Yun and Gardner [23]. Furthermore, the failure mode predicted numerically for all specimens is web-post buckling (WPB), which agrees with the failure mode observed experimentally. Figure 6 illustrates the comparison between the predicted failure mode and the experimental failure mode for the beam B5 and A5.

The geometric parameters H/d_o, s/d_o and d_o/t_w are those which essentially affect the behaviour of cellular beams. The specimens A2 and A5 present the ratio H/d_o equal to1.26 and 1.64, respectively, and the ratio d_o/t_w equal to 71.4 and 51.8, respectively. The yield stress for both specimens is 416 Mpa. It can be noted that as the ratio H/d_o increases and d_o/t_w decreases, the ultimate load and the initial bending stiffness increase and the deflection at the ultimate load decrease. Similar observations can be made for the specimens B1, A6 and B6 for which the H/d_o ratio is equal to 1.26, 1.63 and 1.67, respectively.

Overall, on the basis of data presented in this and previous sections, it can be concluded that the FE model adopted is capable of providing an accurate prediction of the behaviour of steel cellular beams in terms of buckling shear load, load-displacement response and failure mode. There are some small differences in terms of initial bending stiffness, but this is most likely due to localised yielding in the test or due to the machine compliance, which cannot be

assessed accurately in the numerical model. Therefore, in the following sections, the model is used to investigate the effect of the geometrical and material parameters on the behaviour of cellular beams under analysis.

4. Parametric study

In this section, the validated FE model is used to study the influence of geometrical and material parameters on the structural behaviour of high strength steel cellular beams. These include the steel grade, the depth-to-opening diameter ratio, H/d_o, the opening diameter-web thickness ratio, d_o/t_w, and the opening spacing-to-opening diameter, s/d_o. A large number of numerical simulation have been conducted to investigate the effect of each of these parameters on the ultimate load or buckling shear load, on the deflection corresponding to the ultimate load, on the initial bending stiffness, on the failure mode (WPB or VB) and on the post-buckling behaviour. The beams B2 and B6 with H/d_o= 1.25 and 1.67, respectively, are used for this parametric study. The members are assumed to be simply supported with a single point load with an eccentricity of 20 mm from the mid-span in order to prompt the web-post buckling. Initial imperfection is introduced in the models in the shape of the first buckling mode obtained from the Eigenvalue analysis [24] with a scale factor of H/500 [7]. Five s/d_o ratios in the range of 1.1 to 1.5 are studied with five web thicknesses of 5.1 mm, 5.6 mm, 6.0 mm, 6.6 mm and 7.6 mm. d/t_w ratio varies from 40.13 to 59.80 and d_o/t_w ratio varies from 32.24 to 48 for beams with H/d_o=1.67 and varies from 46.33 to 69 for beams with H/do=1.25. Four steel grades S355, S460, S690 and S960 are used throughout this parametric study.

Multi-linear stress-strain relationship for the normal and high strength steel are considered, as shown in the Figure 3. The elastic modulus of steel is taken as 200 GPa and the stresses and strains limits values shown in the Figure 3 are illustrated in Table 2. Figure 7 shows the graphical representation of the stress-strain of the steel grades used in the Table 2.

4.1 Effect of geometric parameters H/d_o, s/d_o and d_o/t_w

Figures 8a- 8d show the load-deflection relationship of cellular beams with H/d_o=1.67, s/d_o=1.2, 1.4 and with H/d_o=1.25, s/d_o=1.2, 1.4 for S355, S460, S690 and S960 steel grades, respectively. For all members the slenderness ratio d/t_w is chosen to be 59.8 (the web thickness is chosen equal to 5.1mm).

It can be noted from Figures 8a to 8d that as the ratio H/d_o increases, the failure load and initial bending stiffness increase, while the deflection at failure decreases. For instance, for members with s/d_o=1.4, when the ratio H/d_o increases from 1.25 to 1.67, the deflection at the web-post failure load decreases by 45%, 37%, 35% and 33% for members with S355, S460, S690 and S960, respectively. For the same members, when the ratio H/d_o increases from 1.25 to 1.67, the web-post failure load increases by 53%, 60%, 66% and 70% for members with S355, S460, S690 and S960, respectively. As it was expectable, it can be noticed that the use of high strength steel grades in cellular beams tends to lead to higher buckling shear load and lower deflection with respect to those obtained from cellular beams made of normal strength steel when the ratio H/d_o increases. However, it also worth pointing out that, as it is

expectable for an intrinsically non-linear phenomenon, the decrease in deflection and the corresponding increase in the value of the failure load cannot be related linearly.

Figures 9a- 9d show the load-deflection relationship of cellular beams with d_o/t_w=32.24, 40.83 and 48.0 for S355, S460, S690 and S960 steel grades, respectively. For all members the ratio H/d_o and s/d_o is chosen to be 1.67 and 1.2, respectively. One can observe that as the ratio d_o/t_w decreases, the web-post failure load and the corresponding deflection substantially increases while the initial bending stiffness increases only slightly. For instance, as the ratio d_o/t_w decreases from 48.0 to 32.24, the deflection at the failure load increases by 194%, 158%, 120% and 72% for steel grades S355, S460, S690, S960, respectively, and the web-post failure load increase by 69%, 65%, 72% and 79% for S355, S460, S690 and S960, respectively. It can be noticed that the employment of high strength steel grades leads to higher buckling shear capacities and lower deflections with respect to normal steel when the ratio d_o/t_w decreases.

Figures 10 and 11 illustrate the bucking shear load for members with s/d_o varies from 1.1 to 1.5 and with d_o/t_w varies from 32.24 to 69 for normal and HS steel. The results are obtained for members with H/d_o=1.67 and H/d_o=1.25, respectively. It can be noticed that the buckling shear load and the failure mode (web-post buckling or Vierendeel failure, see Figure 12) are significantly affected by the geometrical parameters H/d_o, s/d_o and d_o/t_w , and by the steel grade. The bucking shear load increases with increasing ratios s/d_o and H/d_o, as well as with increasing yield stress, and with a decrease of the ratio d_o/t_w. The observed mode of failure for all member with H/d_o=1.67 is web-post buckling while the Vierendeel failure is observed in some members with H/d_o=1.25, particularly for the beams with s/d_o=1.5 and with high ratio of d_o/t_w and with low yield stress (i.e. S355) while the use of HS steel shifts the failure mode into the web-post buckling and provides higher failure loads. This is due to the fact that the web-post is characterised by an increment in the width, thickness and yield stress.

From Figures 10 and 11 one can observe that HS steel provides higher web-post buckling capacities than those provided by normal strength steel. Based on the analysis of the whole cellular beams members used in the parametric study (i.e. beams with H/d_o=1.67 and 1.25) with S355, S460, S690 and S960 steel grades, it is found that the buckling shear load for members with S460, S690 and S960 increases by 20%, 60% and 100% on average compared to the cellular beams made from normal steel S355.

Overall, all the parametric studies show that the results derived from adopting HS steels cannot be linearly extrapolated from the increment in the value of the yielding stress and for such a reason, as it will be shown in the Section 5, design formulae need to be based on a critical analysis of the failure mechanism.

4.2 Effect of high strength steel grade on the stress distribution at the web-post

Figure 13 illustrates the Von-Mises stress distribution at the failure load of cellular beam with H/d_o=1.67, s/d_o =1.2 and d_o/t_w=40.83 made from normal and high strength steel. Only the stress zones that exceed the yield value are shown. As anticipated in the literature, the compressive and tensile stresses tend to act across the web-post on opposite diagonals in order to transmit shear forces and the compressive stress tends to give origin to the web-post

buckling. It can be noticed that the yielding region of the web-post increases as the yield stress of steel increases. For S690 or S960 HS steel, the yielding region evolves over the whole web-post while the yielding region is localised at the ends of the web-post for the S355 normal strength steel. It worth noticing that no yielding region is observed at the middle of the web-post. This suggests that the ideal compressed diagonal strut buckles, as it is shown by the FE analyses, with a two-wave buckling mode, see Figure 14.

5. A discerning model for Web-Post buckling design.

Despite a number of works in the past few years, there is still no consensus about the design procedure for the shear resistance determination and the results obtained by various authors present significant differences when compared with each other, especially when the geometrical parameters become differ from the most used ones. This fact becomes even more evident when the existent models are applied to HS steel cellular beams.

For this reason, a simple mechanical model for the WPB failure is developed and analysed on the basis of geometrical and mechanical parameters in order to highlight the factors which influence the occurrence and the development of the WPB both in normal and HS steels. The procedure is essentially based on the shear model by Ritter and Mörsch, which is also at the basis of the procedure proposed by Lawson et al. [9] but, differently from other methods, does not make reference to code prescriptions and focuses on some key parameters which have not been highlighted before.

Thus, in the present section reference is made first to a simplified model for web-post buckling based on the elementary model of an ideal inclined compressed strut of Figure 15, in analogy of the one suggested by Lawson et al. [9].

The difference here is that the modelling is based only on geometrical and mechanical considerations, without making any reference to code prescriptions or design curves. In this manner the underlying mechanics of the phenomenon can be highlighted and the level of approximation precisely assessed with respect to the numerical models.

The adopted model is founded on the so-called classical truss analogy developed by Ritter and Mörsch. The analogy is thus based on a truss model with parallel chords and web members connected by means of pin joints, where the compressed inclined strut is inclined at a certain angle α' with respect to the longitudinal axis of the cellular beam, see Figure 15.

The value of the force Q is given by

$$Q = \frac{\Delta M}{H - t_f} \tag{1}$$

where

$$V = \frac{\Delta M}{s} \tag{2}$$

$$Q_c = \frac{Q}{2\cos\alpha'} \tag{3}$$

so that

$$V = 2\frac{Q_c}{s}\left(H - t_f\right)\cos\alpha' \tag{4}$$

being M and V the bending moment and the vertical shear buckling load acting on the cellular beam, respectively.

The inclination α' of the ideal compressed strut depends on both geometrical and mechanical factors. In fact, the position of the web holes and their dimensions define the angle α , as shown in Figure 16,

The angle α and the indicated length l_o can be easily derived with reference to Figure 17.

It is

$$\mathrm{a} = \sqrt{\left(R + \frac{s_o}{2}\right)^2 - R^2} = \sqrt{Rs_o + \frac{s_o^2}{4}} \tag{5}$$

$$\alpha = \sin^{-1}\frac{R}{R + \frac{s_o}{2}} \tag{6}$$

and, since $R=d_o/2$,

$$l_o = \frac{d_o}{\sin\alpha} = d_o + s_o \tag{7}$$

The width of the ideal strut b defines the inclination angle α' as a function of α as shown in Figure 18:

Thus, with reference to Figures 17 and 18, it is

$$\frac{\frac{1}{2}\sqrt{b^2 + 4Rs_o + s_o^2}}{\sin\beta} = \frac{R + \frac{b}{2}}{\sin\alpha'} \tag{8}$$

$$\beta = \frac{\pi}{2} - \alpha \quad \rightarrow \quad \sin\beta = \sin\left(\frac{\pi}{2} - \alpha\right) = \cos\alpha \tag{9}$$

$$\alpha' = \sin^{-1}\left(\frac{R+\frac{b}{2}}{\frac{1}{2}\sqrt{b^2+4Rs_o+s_o^2}}\cos\alpha \right) \tag{10}$$

$$l'_o = \frac{R\sqrt{b^2+4Rs_o+s_o^2}}{\left(R+\frac{b}{2}\right)\cos\alpha} \tag{11}$$

So far, all the formulae have been derived from purely geometrical consideration and it is worth noticing that the length of the ideal strut, l'_o, results function of the length l_o of Figure 16, of the inclination angle α and of the width of the strut, b. This is different from all the models in literature, which do not make the inclination of the ideal strut function of its effective width, which is generally assumed as half the web-post width at the mid-height, $s_o/2$ (e.g. [4, 7]) , even if it is widely accepted that the band width in a narrow web-post is significantly wider than this approximation.

From physical considerations and validation through the analysis of the stress distribution in the web-post that results from the performed numerical analyses, it is here proposed that the width of the ideal strut is proportional to the ratio between the actual area of the web-post and the total height of the section, H, see Figure 19.

$$b = \frac{\left[H\left(d_o+s_o\right)-\frac{\pi}{4}d_o^2\right]}{\gamma H} \tag{12}$$

with $\gamma = 6$.

At this point the buckling load Q_c in Equation (4) can be directly derived by the Euler's formula for the buckling of a simple strut,

$$Q_c = \frac{n^2\pi^2 E_t b t_w^2}{12\left(\xi l'_o\right)^2} \tag{13}$$

where E_t is the tangent modulus of the material at the buckling stress and n=2 for the typical two-waves web-post buckling mode found in both the numerical and experimental analyses.

The use of tangent, secant or reduced moduli for the buckling of structures in the plastic range might turn to be rather an intricate matter, depending on the particular case at hand (see, for example, [25-28]) and it has been object of debate for over one century since the first work by Engesser back in 1895. Here reference is made to the stress-strain curves

discussed by Yun and Gardner [23] and to the analysis of tangent and secant moduli proposed by Guarracino and Simonelli [29], so that the equivalent tangent moduli of 50, 60, 80, 100 Gpa are used for S355, S460, S690 and S960, respectively.

However, the calculation of the buckling load Q_c from Equation (13) and, consequently, of the maximum shear load V from Equation (4), requires also the definition of the coefficient ξ and of the effective length l_o' of the ideal Euler's strut.

This because both the geometrical lengths l_o and l_o' in Equations (7) and (11) have been derived from purely geometrical considerations, starting from what is indicated in Figure 16. In reality, the actual length l_o' of the ideal Euler's strut will extend past the region delimitated by the web holes and the strut will also be subject to some form of restrain due to the continuity of the web.

It is worth recalling that Lawson et al. [9] suggested that the effective length of the strut can be assumed equal to half of the diagonal distance across the web-post

$$l_e^{Lawson} = 0.5\sqrt{s_o^{\,2} + d_o^{\,2}} \tag{14}$$

The vertical shear buckling force is given by

$$V = V_h \frac{(H - 2y_t)}{s} \tag{15}$$

where y_t is the depth of the elastic neutral axis of tee from the outer face of the flange (Figure 20), and V_h is horizontal shear force,

$$V_h = \sigma_c \, s_o t_w \tag{16}$$

According to Lawson and Hicks [30] σ_c is the buckling strength obtained from the relevant buckling curve c of Eurocode 3 [10].

However, Lawson's effective length model underestimates the predicted shear strength for narrow web-posts, therefore, Panedpojaman et al. [7] suggested an alternative effective length model as the length between the mid-height and the point of tangency

$$l_e^{Panedpojaman\,(a)} = 0.5\sqrt{s^2 - d_o^{\,2}} \tag{17}$$

Furthermore, Panedpojaman et al. [7] suggested an additional coefficient for the effective length (k) that takes into consideration the tee height that restrains the buckling

$$l_e^{Panedpojaman\,(b)} = k \, l_e^{Panedpojaman\,(a)} \tag{18}$$

with

$$k = 0.9\frac{s}{d_o}\left(\frac{d_o}{d}\right)^2 \le \min\left(1.15\frac{d_o}{d}, 1.15\right) \tag{19}$$

Here, without loss of generality and once again on the bases of the analyses of the results from the performed numerical analyses, it is proposed that

$$l_o' = \frac{H + d_o}{2} \frac{1}{sin\,\acute{\alpha}} \tag{20}$$

similarly to Equation (7) and (10), with

$$\xi = \psi \frac{t_w}{H} \tag{21}$$

by setting $\psi = 20$, the proposed formulation yields the results for the performed analyses which are illustrated in the following Tables.

The predicted buckling shear strength of web-post are based on three effective length models l_e^{Lawson}, $l_e^{Panedpojaman\,(a)}$ and $l_e^{Panedpojaman\,(b)}$ for the models by Lawson et al. [9] and by Panedpojaman et al. [7], using the Equation (15), and on the proposed procedure. All the calculations are made for normal and high strength steel grades. The analytical buckling shear strength of web-post is compared with the numerical buckling shear strength to validate the effective length model and to assess the capability of the design provision explained above. Again the beams B2 and B6 are chosen for this comparison where the ratios s/d_o varies in the range of 1.1 to 1.5 and the ratio d/t_w varies from 40.13 to 59.80. Four steel grades S355, S460, S690 and S960 are taken into consideration.

Table 3 and Table 4 illustrate the ratio between the calculated shear strength V using three effective length models, l_e^{Lawson}, $l_e^{Panedpojaman\,(a)}$ and $l_e^{Panedpojaman\,(b)}$ and the proposed model, and the FE shear strength V_{FE} for S355 and S460 steel. For small values of H/d_o and s/d_o (i.e. H/d_o=1.25 and s/d_o<1.3), $l_e^{Panedpojaman\,(b)}$ overestimates the shear buckling results by up to 44% and 35% for steels S355 and S460, respectively, while it overestimates the shear buckling results by up to 26% for both S355 and S460 and for high values of H/d_o and s/d_o (i.e. H/d_o=1.67 and s/do> =1.3). The overestimation yielded by $l_e^{Panedpojaman\,(b)}$ increases with larger values of slenderness d/t_w. Similarly, $l_e^{Panedpojaman\,(a)}$ overestimates the shear buckling results by up to 59% and 59% and 52% for S355 and S460, respectively, for beams with small values of H/d_o and s/d_o (i.e. H/d_o=1.25 and s/d_o<=1.3). On the other hand, l_e^{Lawson} provides predictions which underestimate the load capacity by up to 63% and 65% for smaller values of s/d_o (i.e. s/d_o=1.1, 1.2) and by up to 30% and 37% for high values of s/d_o (i.e. s/d_o>=1.3) except for some cases, i.e. H/d_o=1.25, d/t_w=40.13 and s/d_o>=1.2 for S355 and s/d_o=1.5 for S460 where only a slight overestimation is found.

When H/d_o =1.67 and s/d_o =1.1, the proposed formulation underestimates the shear buckling by up to 49% and 46% for steel S355 and S460, respectively. However, the proposed formulation results in good agreements with FE shear buckling for beams with H/d_o =1.67 and s/d_o >1.1. For beams with H/d_o =1.25 and s/d_o =1.2, the proposed formulation overestimates the predictions by up to 31% and 29% for steel S355 and S460, respectively. Similarly, the proposed formulation overestimates the predictions for beams with H/d_o =1.25,

s/d_o =1.3 and d/t_w=59.8, 54.46 and 50.83 by up to 23% and 28% for steel S355 and S460, respectively. However, the it provides good agreements with FE shear buckling for H/d_o =1.25 and s/d_o =1.1, 1.4, 1.5.

Tables 5 and 6 show the ratio between the calculated shear strength V and the FE shear strength V_{FE} using three effective length models l_e^{Lawson}, $l_e^{Panedpojaman\,(a)}$ and $l_e^{Panedpojaman\,(b)}$ and the new proposal for S690 and S960 high strength steel. $l_e^{Panedpojaman\,(b)}$ overestimates the shear buckling in some cases by up to 21% and 26% when d/t_w=40.13 and up to 10% and 9% when H/d_o=1.67 and s/d_o=1.2, 1.3.

On the other hand, the predicted shear buckling for S690 and S960 obtained using l_e^{Lawson} is underestimated by up to 72% and 76% for smaller values of s/d_o (i.e. s/d_o=1.1, 1.2) and for larger s/d_o (i.e. s/d_o=1.3, 1.4, 1.5) the results are underestimated by up to 48% and 55% for S690 and S960, respectively.

When H/d_o =1.67 and s/d_o =1.1, the proposed formulation underestimates the shear buckling by up to 47% and 46% for steel S690 and S960, respectively. However, the proposed procedure results in good agreements with FE shear buckling for beams with H/d_o =1.67 and s/d_o >1.1. For beams with H/d_o =1.25 and s/d_o =1.2, the proposed formulation overestimates the predictions by up to 31% and 29% for steel S690 and S960, respectively. Similarly, the proposed formulation overestimates the predictions for beams with H/d_o =1.25, s/d_o =1.3 and d/t_w=59.8, 54.46 and 50.83 by up to 23% and 28% for steel S690 and S960, respectively. However, the it provides good agreements with FE shear buckling for H/d_o =1.25 and s/d_o =1.1, 1.4, 1.5.

Overall, the proposed analytical formulation results in better agreement with the FE results for the whole range of investigated geometries and both for normal and HS steel. This can be essentially attributed to the ability to adapt both the width and the inclination of the compressd ideal strut to the geometry of the case, see equations (12) and (20), respectively.

Figures 21 shows a graphical representation of all the analytically predicted and FE calculated shear strength for beams made from mild and HS steel. It can be seen that the use of $l_e^{Panedpojaman\,(a)}$ or $l_e^{Panedpojaman\,(b)}$ as effective buckling length in the calculation of shear buckling using nominal buckling equations of BS EN 1993-1-1 generally tends to overestimate the predicted buckling shear strength of cellular beams for both normal and high strength steel. The use of l_e^{Lawson} tends to provide acceptable predictions for the normal strength steel and very conservative predictions for HS steel, especially for the S960.

Table 7 illustrate the calculated root-mean-square (RMS) errors for the predicted shear strength V using three effective length models, l_e^{Lawson}, $l_e^{Panedpojaman\,(a)}$ and $l_e^{Panedpojaman\,(b)}$ and the proposed model, for both normal and high-strength steel. The RMS error is defined as

$$\text{RMS error} = \sqrt{\frac{\text{SSE}}{\text{n}}} \qquad (22)$$

Where n is the number of data points over which the sum of the squared error SSE between the finite-element shear strength V_i^{FE} and the predicted shear strength $V_i^{pred.}$, given as:

$$SSE = \sum_{1}^{N} \left(V_i^{FE} - V_i^{pred.} \right)^2 \quad (23)$$

It can be pointed out that the RMS error ranges between 18.5 and 37.7 for the shear strength predicted by the proposed formulation while it ranges between 21.8 and 49.1 for the shear strength predicted by $l_e^{Panedpojaman\,(b)}$, between 21.8 and 59.7 for the shear strength predicted by $l_e^{Panedpojaman\,(a)}$ and between 29.3 and 99.5 for shear strength predicted by l_e^{Lawson}.

Thus, the RMS error for the predicted shear strength V according to the proposed model results on average lower than the ones relative to the use of the effective length models l_e^{Lawson}, $l_e^{Panedpojaman\,(a)}$ and $l_e^{Panedpojaman\,(b)}$.

In the end, it is evident that the proposed formulation seems to provide shear buckling results that are in much more reasonable agreement with those obtained by FE analysis for both mild and HS steel.

6. A statistical evaluation in the fashion of Annex D EN 1990

Even if, as stated in the Introduction, the proposed procedure does not make reference to code prescriptions and focuses on the mechanics of the phenomenon only, a statistical analysis in the fashion of the provisions of Annex D EN 1990 (2002) [31] has been carried out in order to assess the reliability of the proposed formulation. However, in the framework of the present study the statistical evaluation of the proposed prediction model is done here against the numerical results.

Tables 8 and 9 below summarise the following key statistical parameters: the number of tests and FE simulations n, the design fractile factor (ultimate limit state), $k_{d,n}$, the average ratio of FE to model resistance based on a least squares fit to all the data, $\bar{b}$, the combined coefficient of variation incorporating both model and basic variable uncertainties, V_r, and the partial safety factor for cross-section resistance γ_{M0}. The material over-strength of high strength steel was taken equal to 1.135 with a coefficient of variation COV of 0.055, while the COV of geometric properties was assumed equal to 0.02 [32]. For normal strength steel, the material over-strength of high strength steel was taken equal to 1.25 with a coefficient of variation COV of 0.055 [33]. The COV between the experimental and the numerical results, which was found equal to 0.025, was also considered. Performing a First Order Reliability Method (FORM) in accordance with the Eurocode target reliability requirements, the partial factors γ_{M0} were evaluated.

It has to be mentioned again that for s/do=1.1 the failure, see Figure 22, is not in the fashion of the typical two waves post buckling shown in Figure 14. Therefore, the reliability analysis has been here performed both considering and not considering the cases s/do=1.1. The results

are collected in Table 1 and 2, respectively, and it is evident that the elimination of the failure modes not modelled by the proposed formulation leads to much more consistent results. It goes without saying that none of the other formulations would be able to cover these atypical cases, either.

Overall, the performed statistical analysis seems to confirm the reliability of the proposed formulation.

7. Conclusions

A comprehensive numerical analysis of the behaviour of cellular beams made from normal and high strength steel with various geometries has been performed and discussed. The finite element models have been developed using commercial software ABAQUS and validated against existing experimental results conducted by Grilo et al. [5] and Tsavdaridis and D'Mello [4].

Since there is currently no unanimous consensus about the design procedure for the shear resistance determination, on the basis of the obtained numerical results a simple mechanical model for the WPB failure has been proposed in order to highlight the factors which influence the occurrence and the development of the WPB both in normal and HS steels.

The resulting analytical formulation results in better agreement with the FE results for the whole range of investigated geometries and both for normal and HS steel, on account of its capability to adapt both the width and the inclination of the compressd ideal strut to the geometry of the case.

As a consequence, it is found that the proposed analytical procedure can be used as basis for the development of a reliable design method to predict shear buckling of web-post of cellular beams made both of mild and HS steel.

Acknowledgements

The first author would like to acknowledge the Centre for Civil and Building Services Engineering at London South Bank University for the encouragement and providing technical supports for this research.

References

[1] Ward, J 1990 Design of Composite and Non-Composite Cellular Beams, 100, The Steel Construction Institute, SCI Publication.

[2] Kuchta, K. and Maślak, M., 2015. Failure modes determining the resistance and the stability of steel cellular beams. Czasopismo Inżynierii Lądowej, *Środowiska i Architektury*, 62(4), 263-280.

[3] Nseir, J., Lo, M., Sonck, D., Somja, H., Vassart, O. and Boissonnade, N., 2012, April. Lateral torsional buckling of cellular steel beams. In Proceedings of the Annual Stability Conference Structural Stability Research Council, 18-21.

[4] Tsavdaridis, K.D. and D'Mello, C., 2011. Web buckling study of the behaviour and strength of perforated steel beams with different novel web opening shapes. *Journal of Constructional Steel Research*, 67(10), 1605-1620.

[5] Grilo, L.F., Fakury, R.H. and de Souza Veríssimo, G., 2018. Design procedure for the web-post buckling of steel cellular beams. *Journal of Constructional Steel Research*, 148, 525-541.

[6] Erdal, F. and Saka, M.P., 2013. Ultimate load carrying capacity of optimally designed steel cellular beams. *Journal of constructional steel research*, 80, 355-368.

[7] Panedpojaman, P., Thepchatri, T. and Limkatanyu, S., 2014. Novel design equations for shear strength of local web-post buckling in cellular beams. *Thin-walled structures*, 76, 92-104.

[8] Fares, S., Coulson, J. , Dinehart, D, 2016 Steel Design Guide 31: Castellated and Cellular Beam Design – AISC, 2016.

[9] Lawson, R.M., Lim, J., Hicks, S.J. and Simms, W.I., 2006. Design of composite asymmetric cellular beams and beams with large web openings. *Journal of Constructional Steel Research*, 62(6), 614-629.

[10] Eurocode, CEN., 2005. 3: Design of Steel Structures, Part 1-1 "General Rules and Rules for Buildings". CEN, Brussels: European Committee for Standardization.

[11] Ricles, J.M., Sause, R. and Green, P.S., 1998. High-strength steel: implications of material and geometric characteristics on inelastic flexural behavior. *Engineering Structures*, 20(4-6), 323-335.

[12] Lee, C.H., Han, K.H., Uang, C.M., Kim, D.K., Park, C.H. and Kim, J.H., 2012. Flexural strength and rotation capacity of I-shaped beams fabricated from 800-MPa steel. *Journal of Structural Engineering*, 139(6), 1043-1058.

[13] Ma, J.L., Chan, T.M. and Young, B., 2016. Experimental investigation of cold-formed high strength steel tubular beams. *Engineering Structures*, 126, 200-209.

[14] Rasmussen, K.J.R. and Hancock, G.J., 1995. Tests of high strength steel columns. *Journal of Constructional Steel Research*, 34(1), 27-52.

[15] Ban, H., Shi, G., Shi, Y. and Bradford, M.A., 2013. Experimental investigation of the overall buckling behaviour of 960 MPa high strength steel columns. *Journal of Constructional Steel Research*, 88, 256-266.

[16] Wang, Y.B., Li, G.Q., Chen, S.W. and Sun, F.F., 2012. Experimental and numerical study on the behavior of axially compressed high strength steel columns with H-section. *Engineering Structures*, 43, 149-159.

[17] Puthli, R. and Fleischer, O., 2001. Investigations on bolted connections for high strength steel members. *Journal of constructional steel research*, 57(3), 313-326.

[18] Može, P., Beg, D. and Lopatič, J., 2007. Net cross-section design resistance and local ductility of elements made of high strength steel. *Journal of Constructional Steel Research*, 63(11), 1431-1441.

[19] Uy, B. and Sloane, R.J., 1998. Behaviour of composite tee beams constructed with high strength steel. *Journal of Constructional Steel Research*, 1(46), 203-204.

[20] Shamass, R. and Cashell, K.A., 2017. Behaviour of composite beams made using high strength steel. In Structures, vol. 12, 88-101. Elsevier.

[21] Ban, H., Bradford, M.A., Uy, B. and Liu, X., 2016. Available rotation capacity of composite beams with high-strength materials under sagging moment. *Journal of Constructional Steel Research*, 118, 156-168.

[22] Uy, B., Khan, M., Tao, Z. and Mashiri, F., 2013. Behaviour and design of high strength steel-concrete filled columns. In Proceedings of the 2013 World Congress on Advances in Structural Engineering and Mechanics (ASEM13), Jeju, Korea, 150-167.

[23] Yun, X. and Gardner, L. 2017. Stress-strain curves for hot-rolled steels. *Journal of Constructional Steel Research*. 133, 36-46.

[24] Abaqus. Reference Manual, Version 6.11. France: Simulia, Dassault Systèmes, 2011.

[25] Shamass, R. Alfano, G. and Guarracino, G., 2014. A numerical investigation into the plastic buckling paradox for circular cylindrical shells under axial compression, *Engineering Structures*, 75, 429-447.

[26] Shamass, R. Alfano, G. and Guarracino, G, 2015. An investigation into the plastic buckling paradox for circular cylindrical shells under non-proportional loading, *Thin-Walled Structures*, 95, 347-362.

[27] Shamass, R. Alfano, G. and Guarracino, G, 2015. An analytical insight into the buckling paradox for circular cylindrical shells under axial and lateral loading, *Mathematical Problems in Engineering*, Article number 514267, doi: 10.1155/2015/514267

[28] Shamass, R. Alfano, G. and Guarracino, G. 2017. On Elastoplastic Buckling Analysis of Cylinders Under Nonproportional Loading by Differential Quadrature Method, *Int J of Structural Stability and Dynamics*, 17 (7), Article number 1750072.

[29] Guarracino, F. and Simonelli, M.G. 2017. The torsional instability of a cruciform column in the plastic range: Analysis of an old conundrum, *Thin-Walled Structures*, 113, 273-286.

[30] Lawson, R.M. and Hicks, S.J., 2011. Design of composite beams with large web openings: in accordance with Eurocodes and the UK National Annexes. *Steel Construction Institute*.

[31] EN 1990. 2002. Eurocode - Basis of structural design (English).

[32] Gkantou, M., Theofanous, M., Antoniou, N. and Baniotopoulos, C., 2017. Compressive behaviour of high-strength steel cross-sections, *Proceedings of the Institution of Civil Engineers-Structures and Buildings, 170(11)*, 813-824..

[33] McCann, F. and Gardner, L., 2019. Numerical analysis and design of slender elliptical hollow sections in bending, *Thin-Walled Structures*, 139, 196-208.

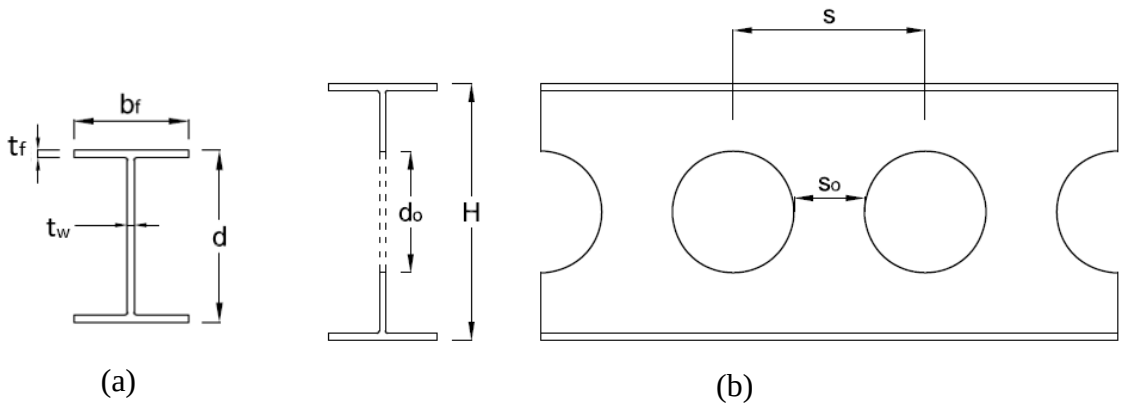

Figure 1: (a) Parent I-beam section; (b) Cellular beam geometry

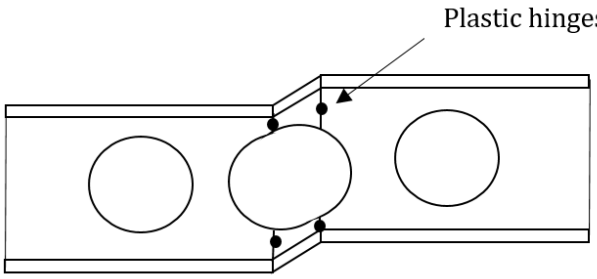

(a)

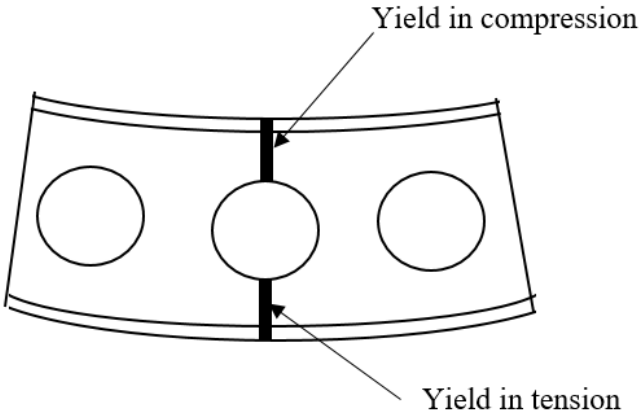

(b)

(c)

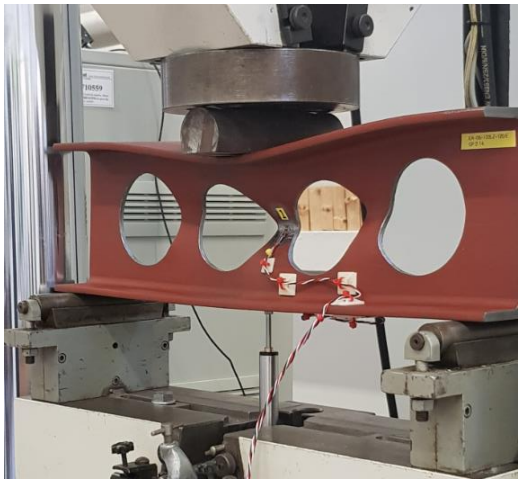

(d)

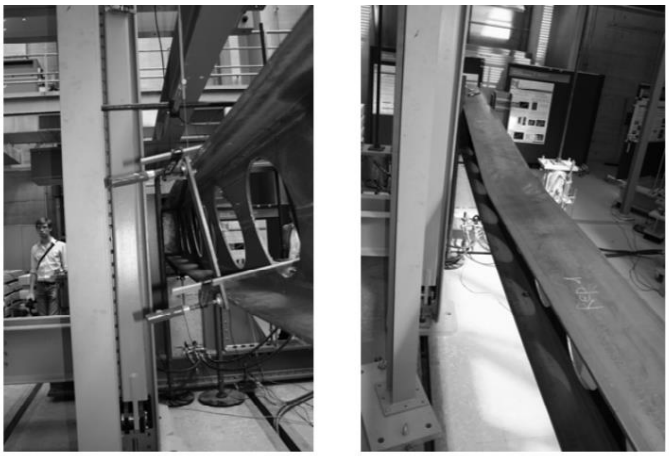

(e)

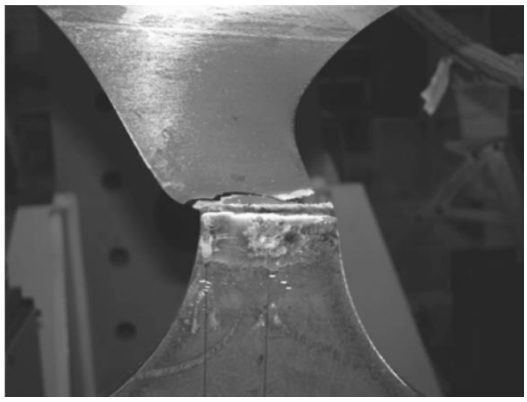

(f)

Figure 2: Some failure modes of cellular beams: (a) Vierendeel bending, VB [1]; (b) overall bending failure, BF [1]; (c) shear failure, SF [2]; (d) web-post buckling WPB; (e) lateral torsional buckling, LTB [3]; and (f) rupture of weld joints [2]

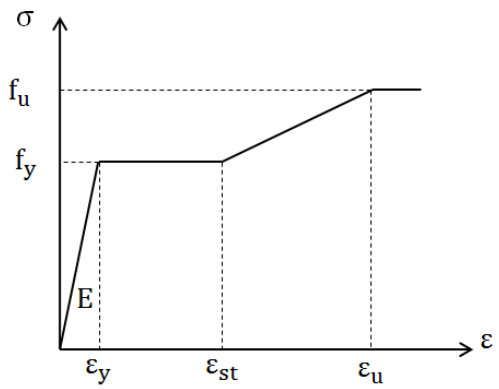

Figure 3: Stress-strain relationship of steel material in cellular beam

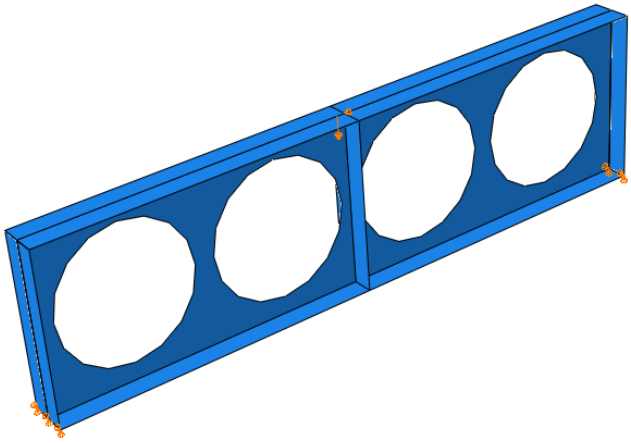

Figure 4: The loading, boundary conditions and geometries of the FE model

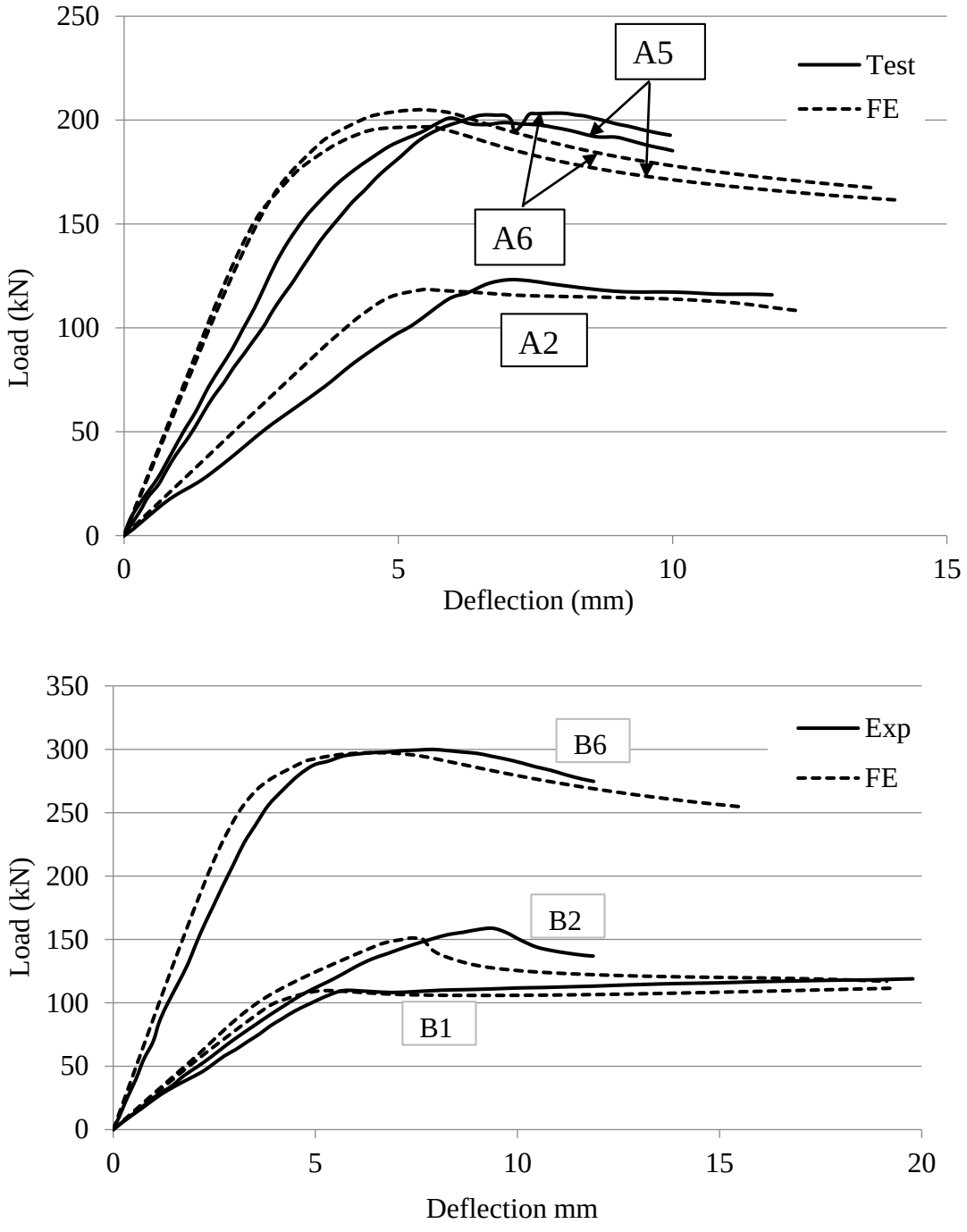

Figure 5: Load-deflection relationship predicted by FE model and obtained experimentally

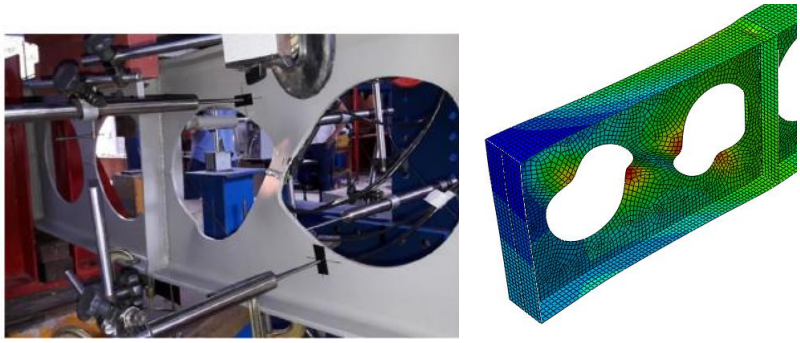

(a)

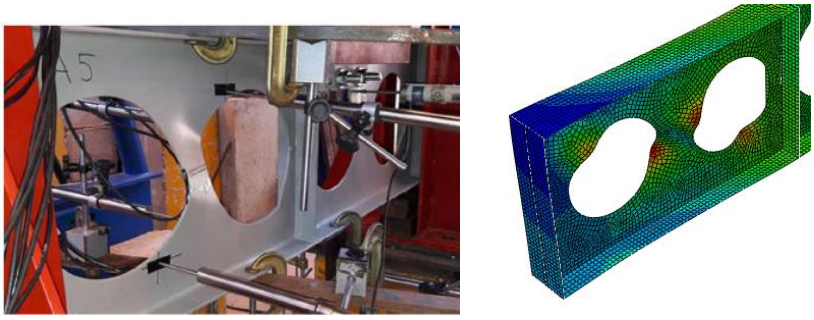

(b)

Figure 6: Comparison between FE and experimental failure mode for (a) B5 and (b) A5

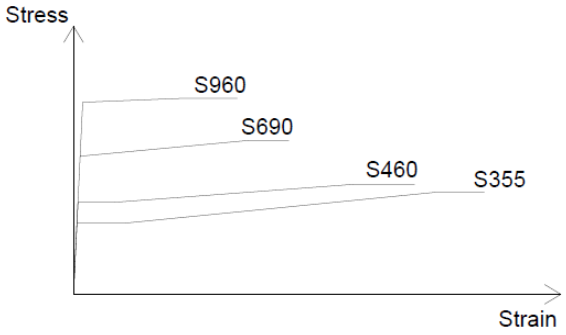

Figure 7: The stress-strain relationship of steel grades used in the Table 2

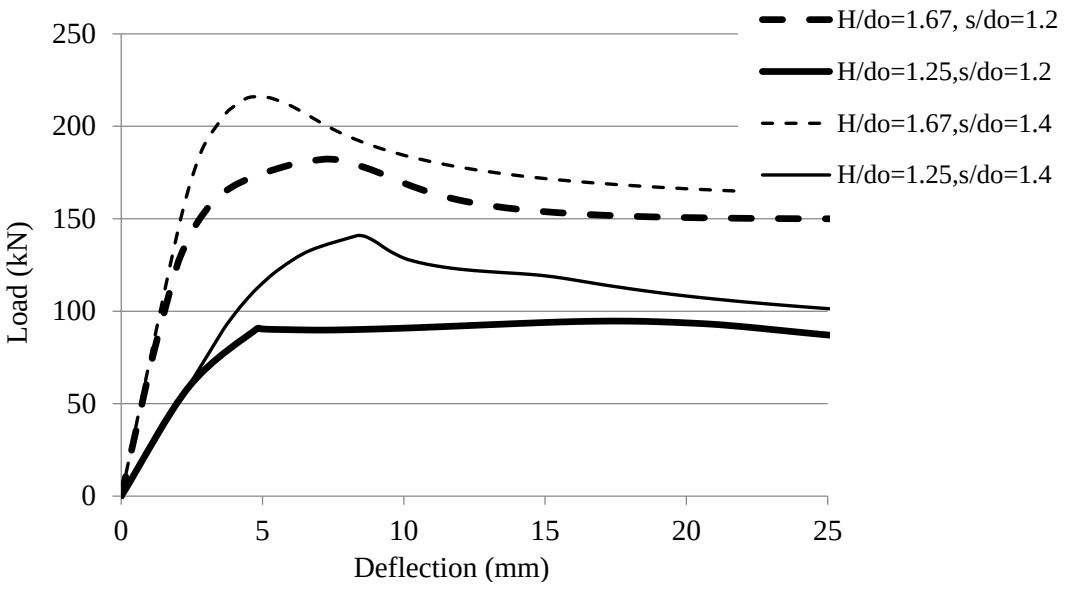
H/do=1.67, s/do=1.2
H/do=1.25,s/do=1.2
H/do=1.67,s/do=1.4
H/do=1.25,s/do=1.4
Load (kN)
Deflection (mm)
0
50
100
150
200
250
0
5
10
15
20
25

(a)

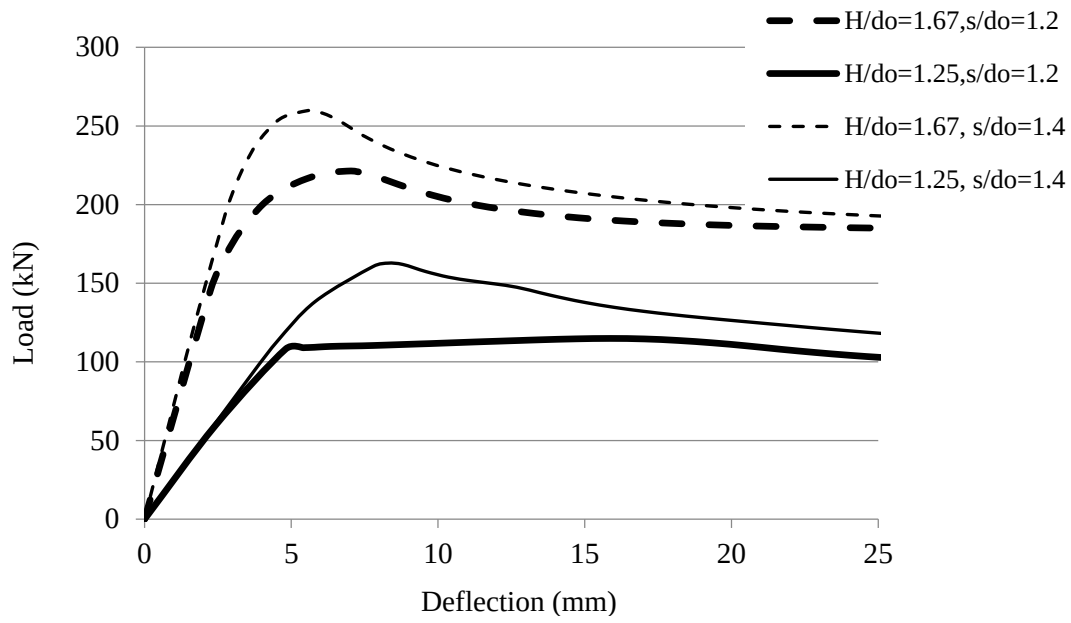
H/do=1.67,s/do=1.2
H/do=1.25,s/do=1.2
H/do=1.67, s/do=1.4
H/do=1.25, s/do=1.4
Load (kN)
Deflection (mm)
0
50
100
150
200
250
300
0
5
10
15
20
25

(b)

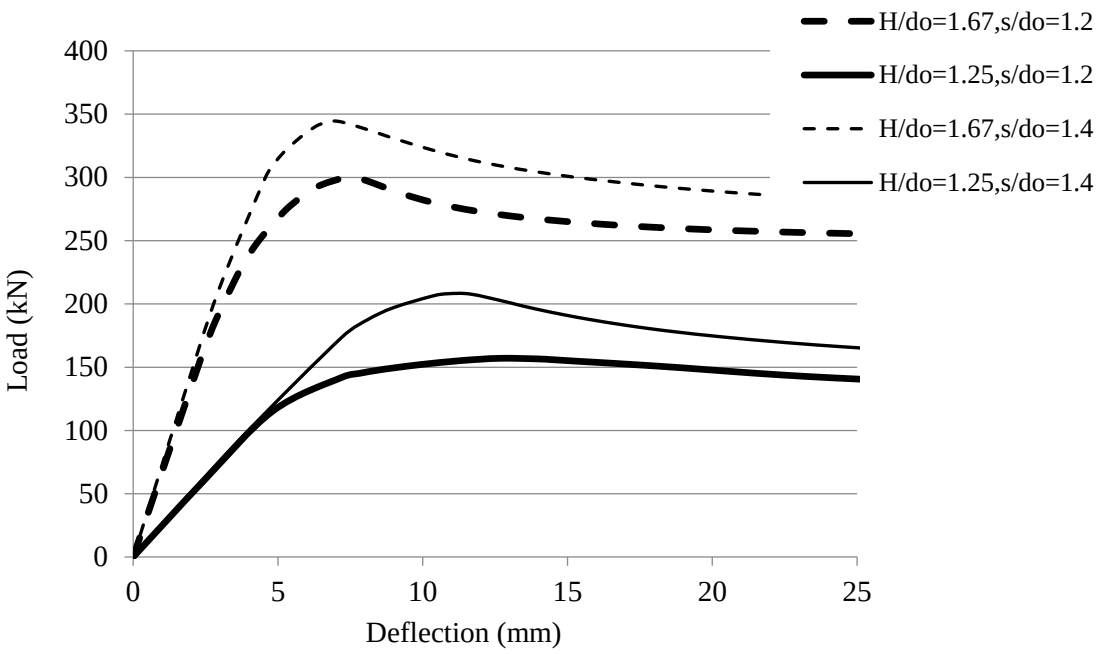

(c)

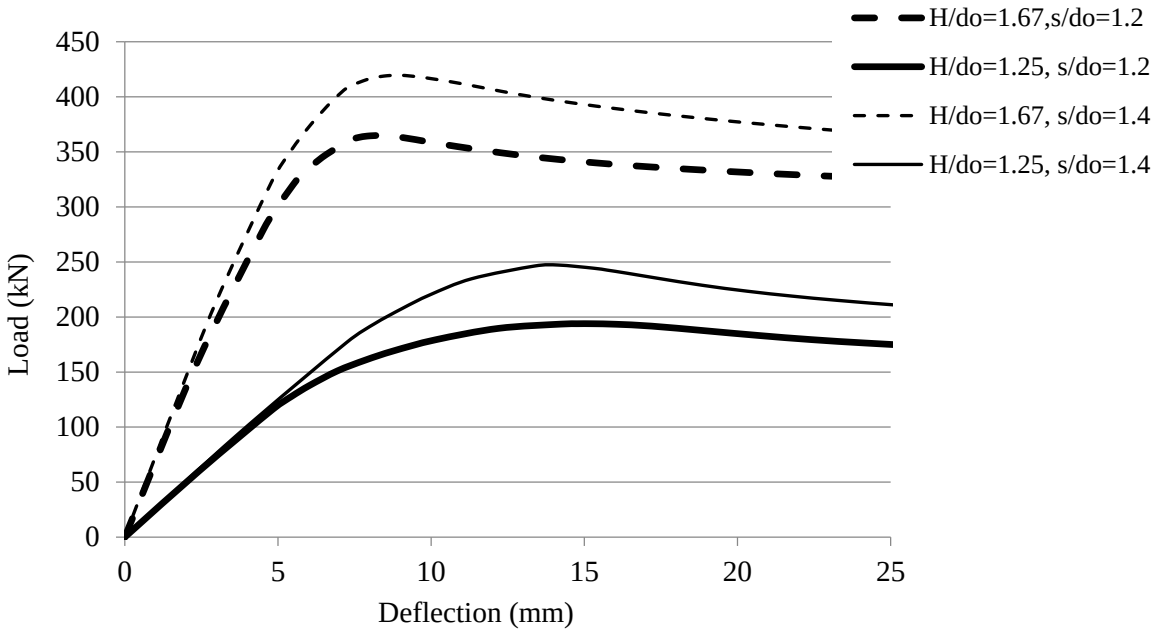

(d)

Figure 8: Load-deflection curves for members made from (a) S355; (b) S460; (c) S690; (d) S960

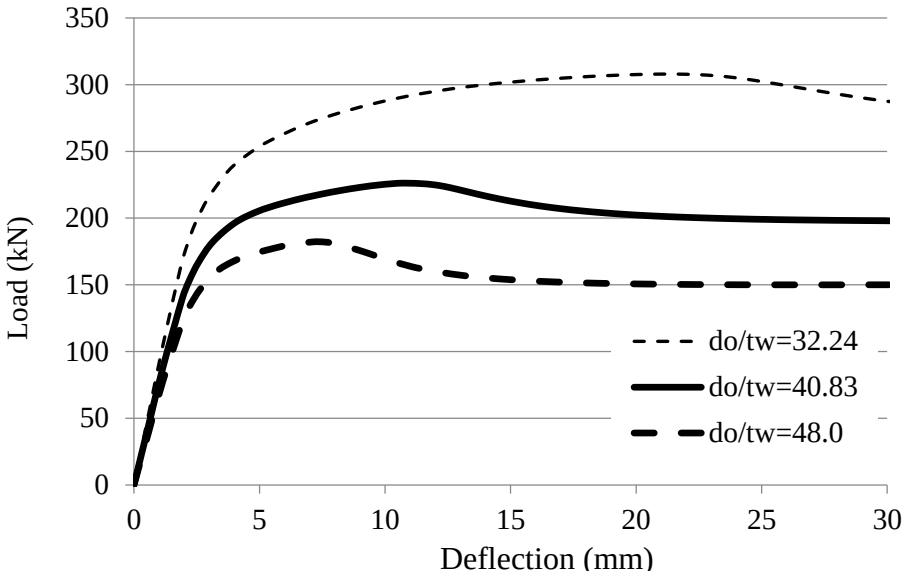
350
300
250
200
150
100
50
0
Load (kN)
0
5
10
15
20
25
30
Deflection (mm)
do/tw=32.24
do/tw=40.83
do/tw=48.0

(a)

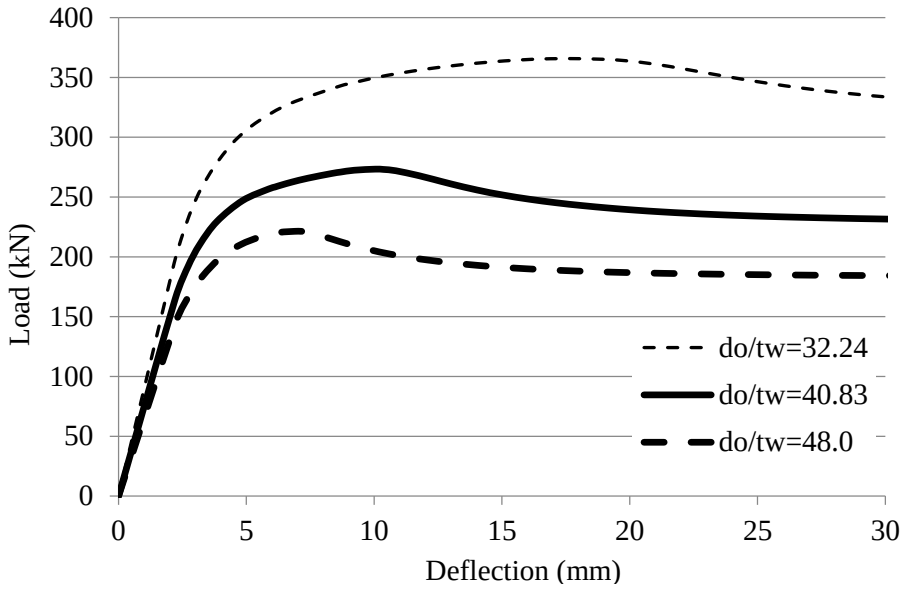
400
350
300
250
200
150
100
50
0
Load (kN)
0
5
10
15
20
25
30
Deflection (mm)
do/tw=32.24
do/tw=40.83
do/tw=48.0

(b)

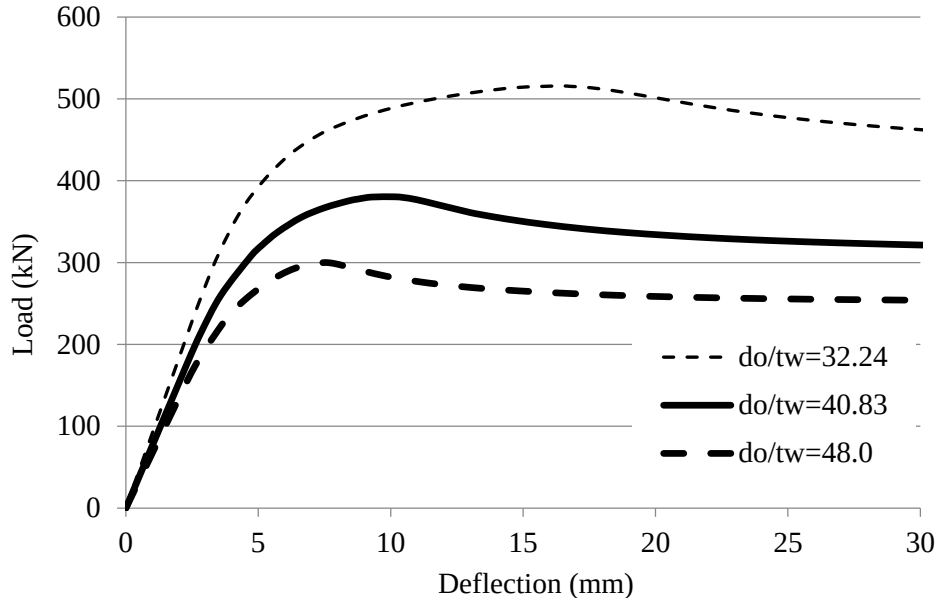

(c)

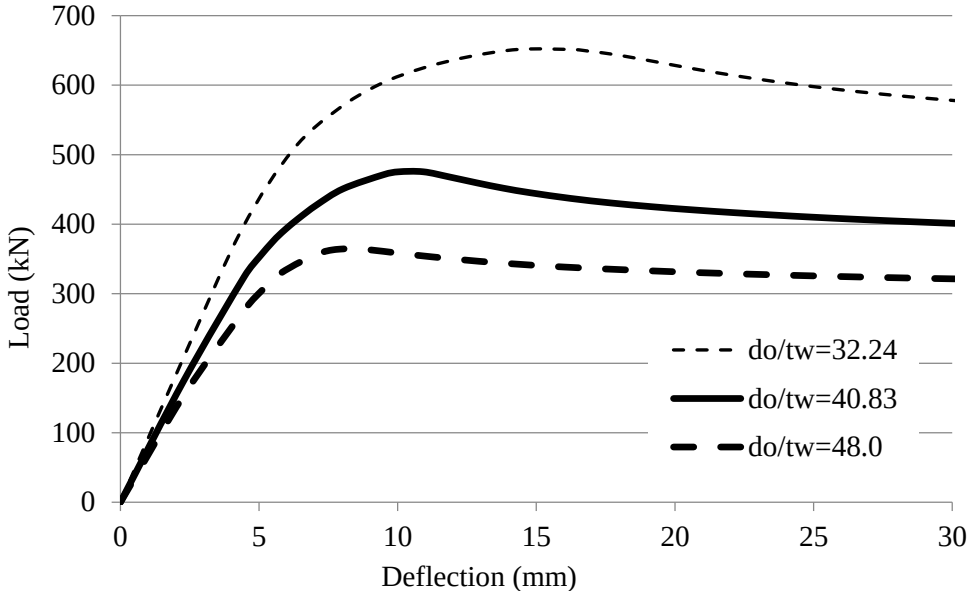

(d)

Figure 9: Load-deflection curves for members with different d_o/t_w ratios and made from (a) S355; (b) S460; (c) S690; (d) S960 (H/d_o and s/d_o is 1.67 and 1.2)

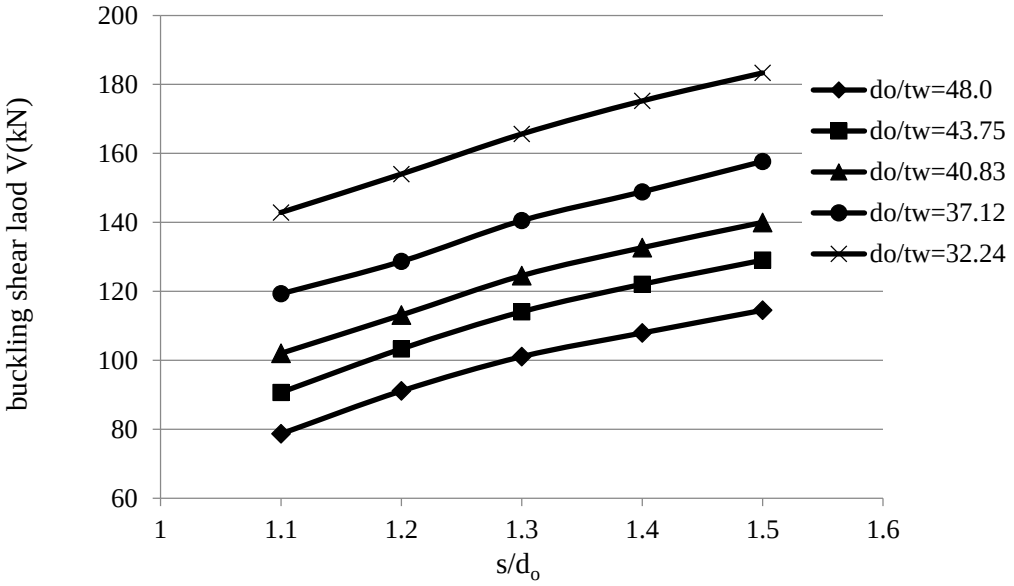
buckling shear laod V(kN)
200
180
160
140
120
100
80
60
1
1.1
1.2
1.3
1.4
1.5
1.6
s/d_o
do/tw=48.0
do/tw=43.75
do/tw=40.83
do/tw=37.12
do/tw=32.24

(a)

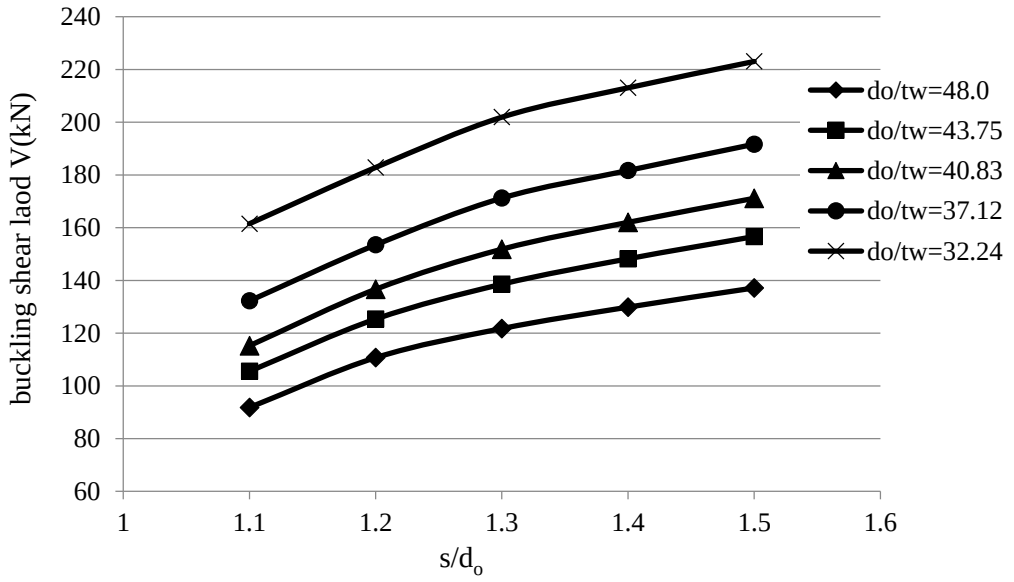
buckling shear laod V(kN)
240
220
200
180
160
140
120
100
80
60
1
1.1
1.2
1.3
1.4
1.5
1.6
s/d_o
do/tw=48.0
do/tw=43.75
do/tw=40.83
do/tw=37.12
do/tw=32.24

(b)

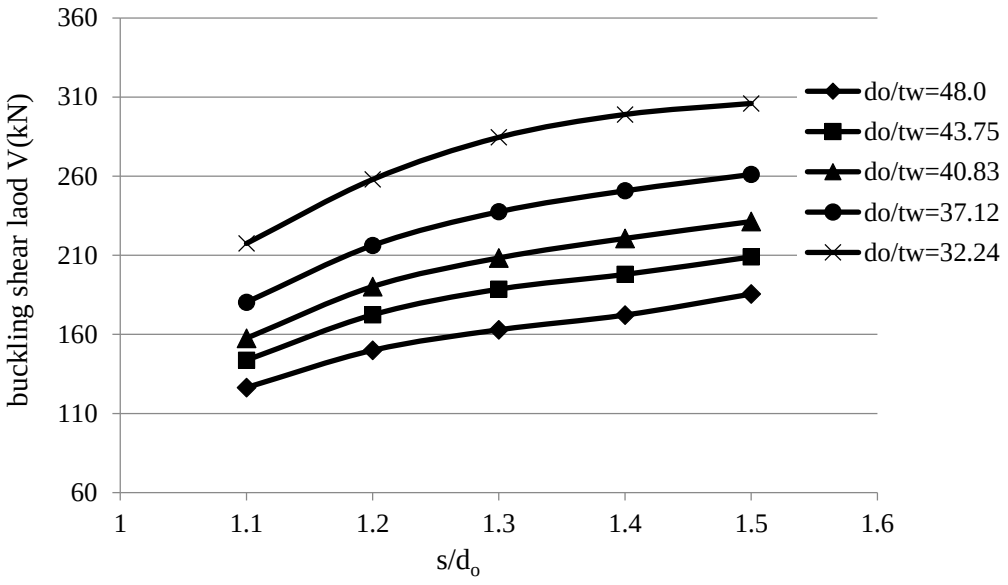

(c)

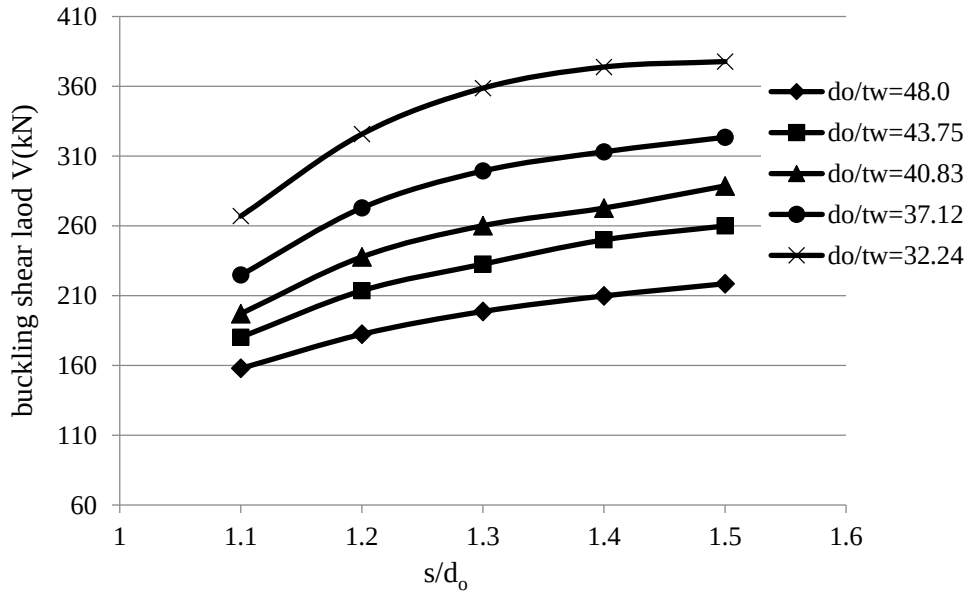

(d)

Figure 10: Influence of s/d_o and d_o/t_w geometrical parameters on the buckling shear load of cellular beams with $H/d_o=1.67$ and made from (a) S355; (b) S460; (c) S690; (d) S960

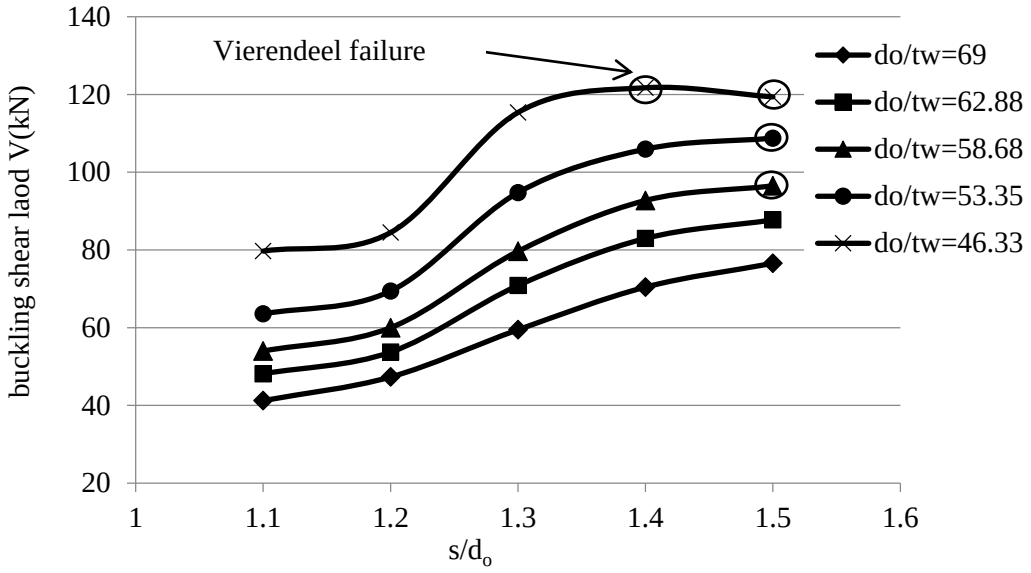
Vierendeel failure
do/tw=69
do/tw=62.88
do/tw=58.68
do/tw=53.35
do/tw=46.33
buckling shear laod V(kN)
140
120
100
80
60
40
20
1
1.1
1.2
1.3
1.4
1.5
1.6
s/d_o

(a)

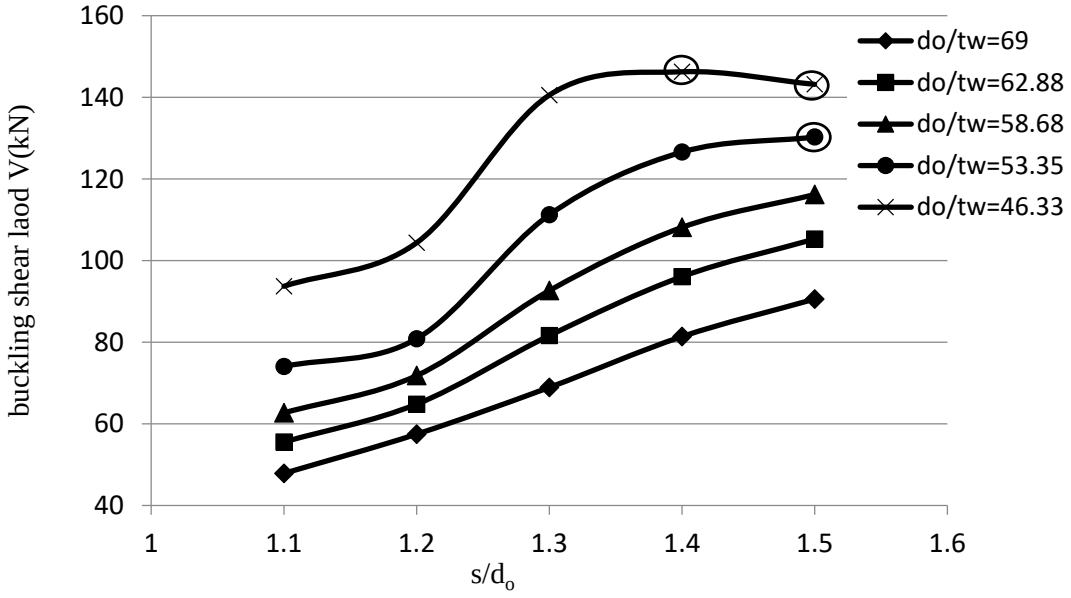
do/tw=69
do/tw=62.88
do/tw=58.68
do/tw=53.35
do/tw=46.33
buckling shear laod V(kN)
160
140
120
100
80
60
40
1
1.1
1.2
1.3
1.4
1.5
1.6
s/d_o

(b)

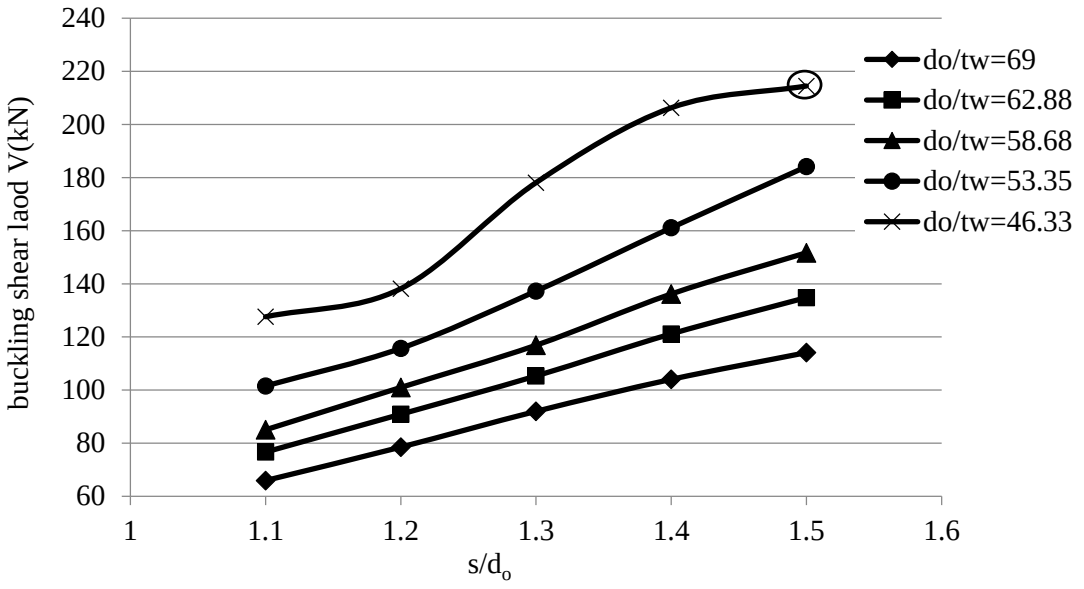

(c)

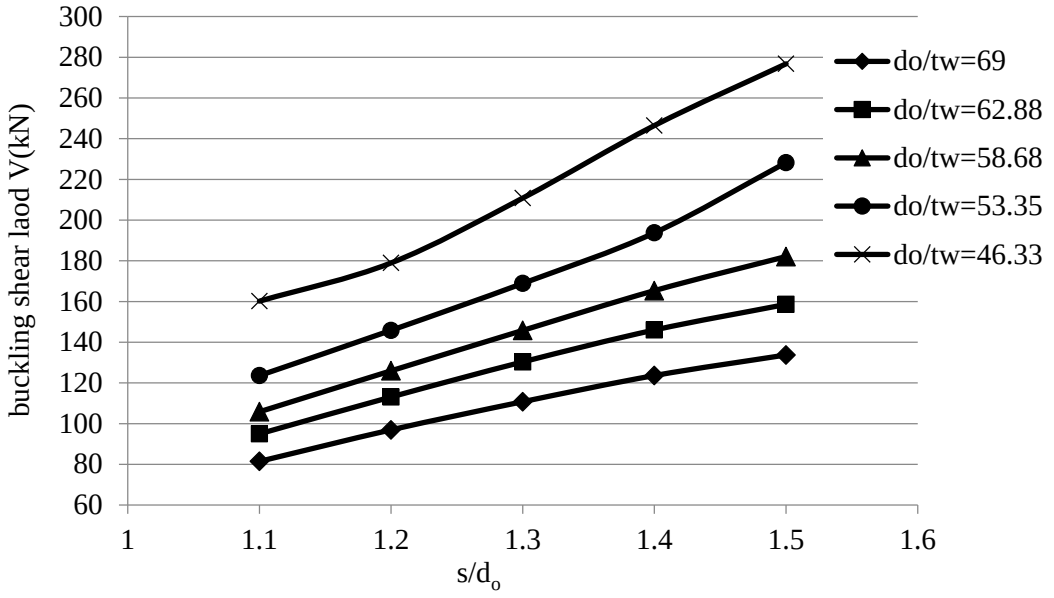

(d)

Figure 11: Influence of s/d_o and d_o/t_w geometrical parameters on the buckling shear load of cellular beams with H/d_o=1.25 and made from (a) S355; (b) S460; (c) S690; (d) S960

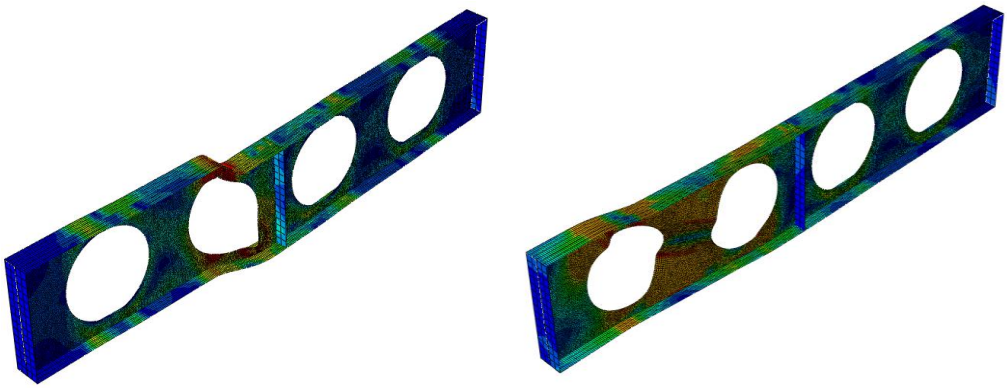

(a) (b)

Figure 12: Observed failure modes of the cellular beams (a) Vierendeel failure; (b) web-post buckling

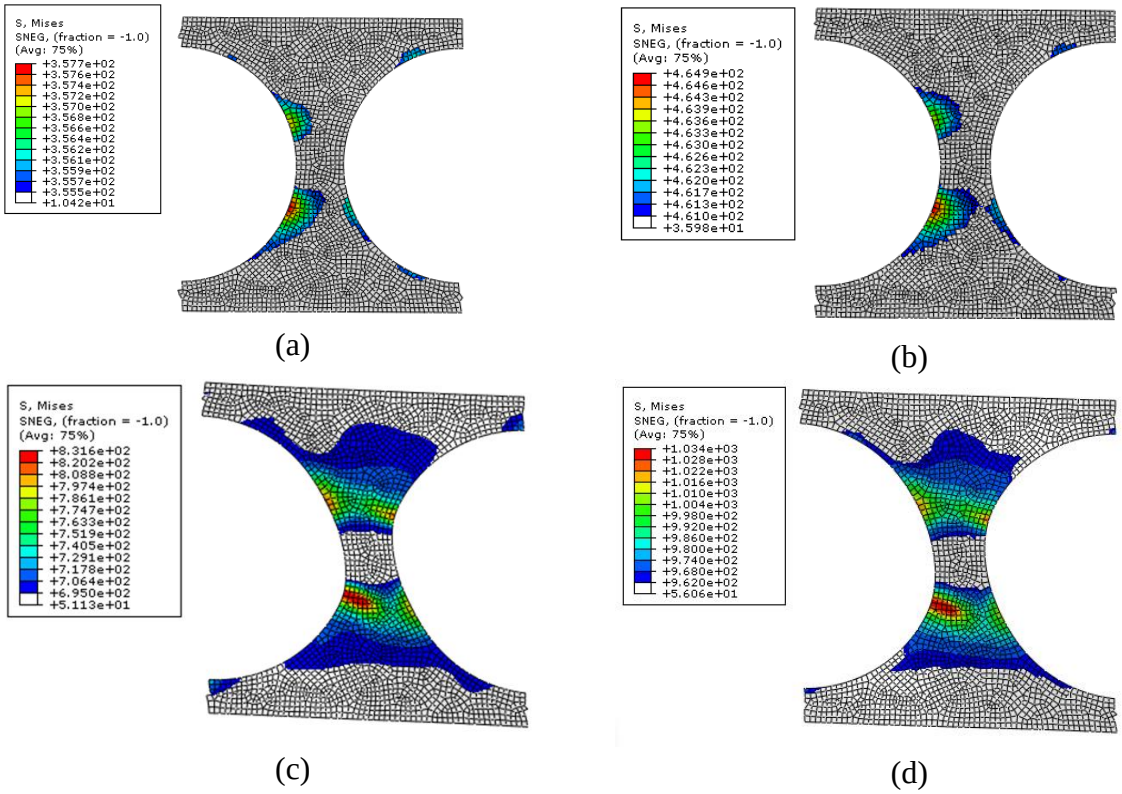

Figure13: The Von-Mises stress distribution at the web-post for (a) S355, (b) S460, (c) S690, (d) S960

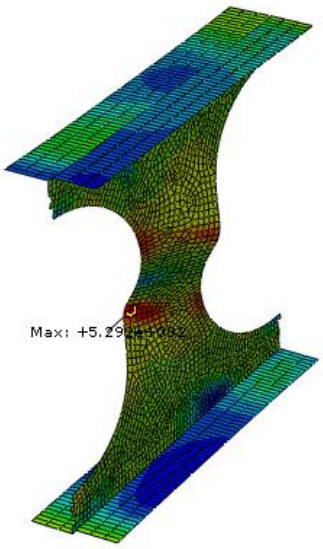

Figure14: Typical two-waves web-post buckling mode.

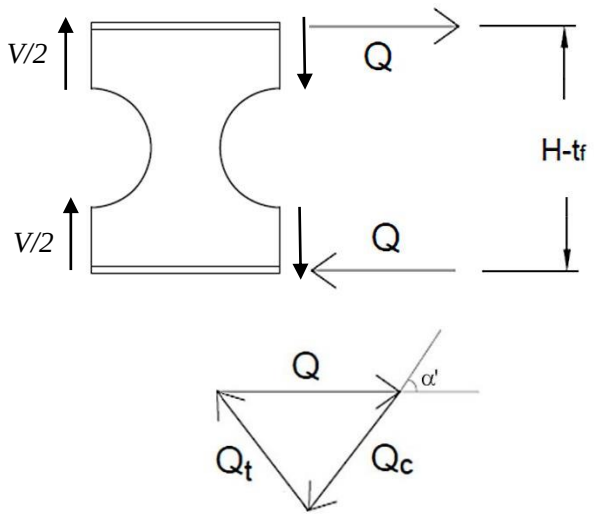

Figure 15: Forces Q acting at the top and bottom flanges and decomposition into components Q_t and Q_c through the web member.

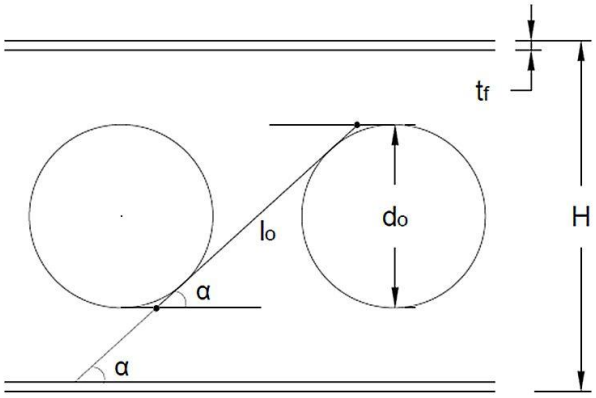

Figure 16: Inclination α of the tangent to the web holes.

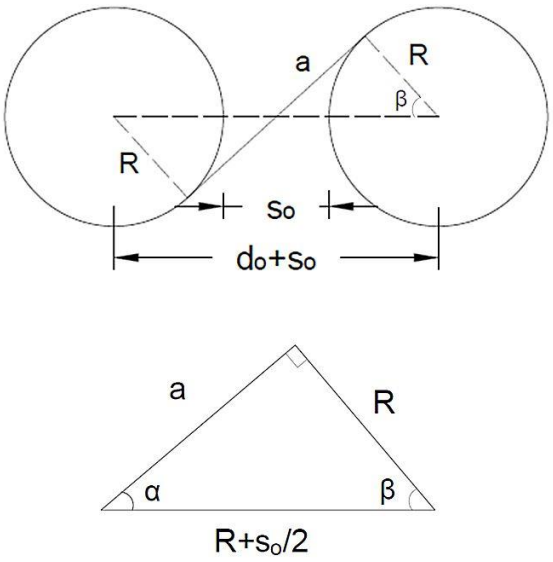

Figure 17: Basic geometric relationships

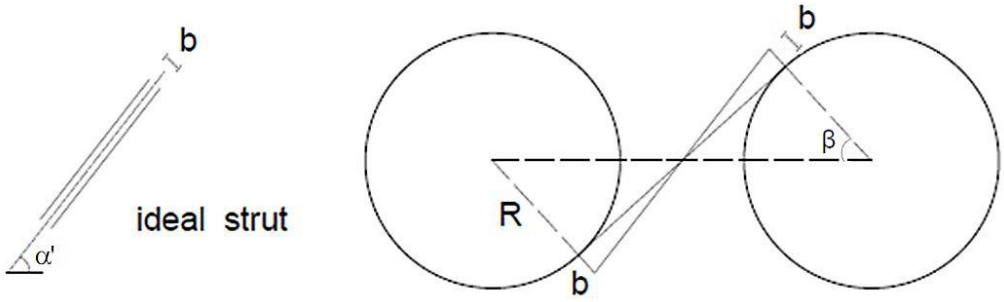

Figure 18: Width of the ideal strut.

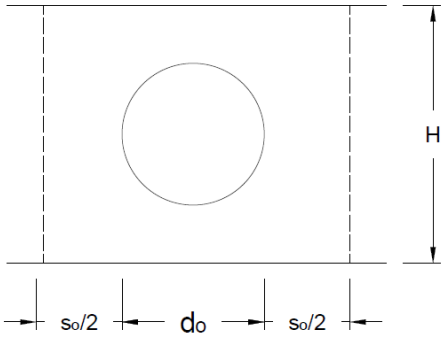

Figure 19: Area of the web-post.

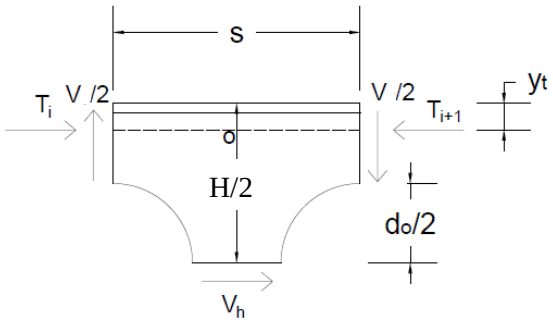

Figure 20: Horizontal shear in the web post of cellular beam

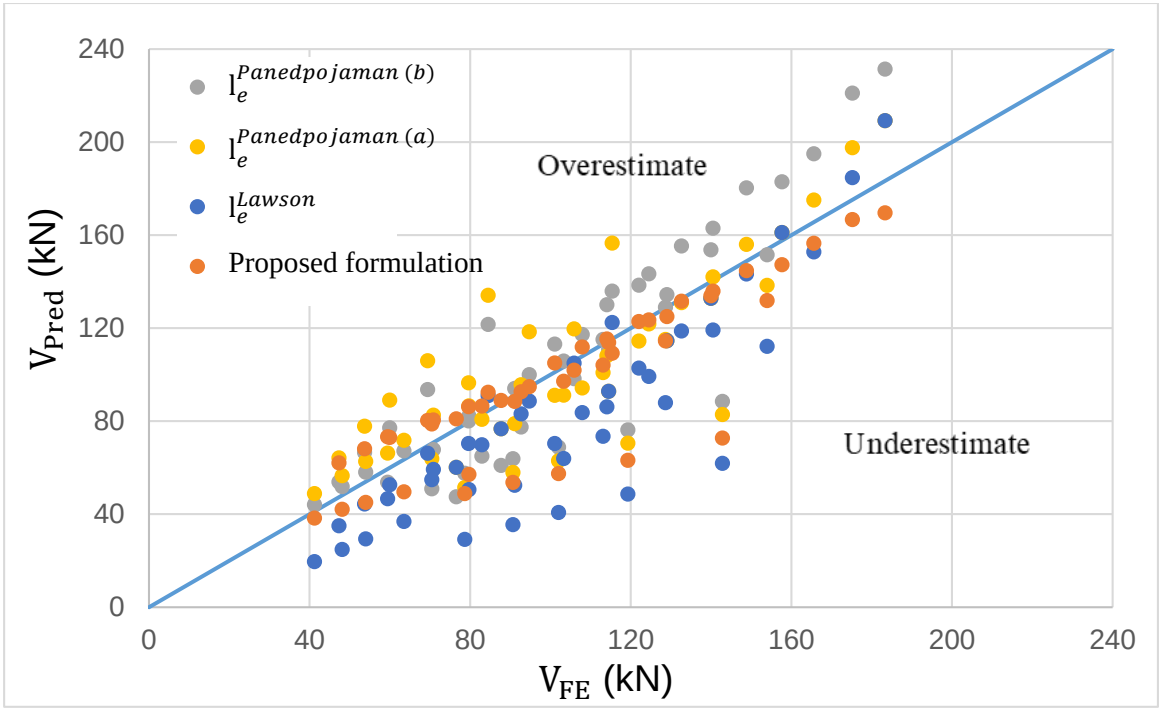
240
200
160
120
80
40
0
0
40
80
120
160
200
240
V_{Pred} (kN)
V_{FE} (kN)
$l_e^{Panedpojaman\ (b)}$
$l_e^{Panedpojaman\ (a)}$
l_e^{Lawson}
Proposed formulation
Overestimate
Underestimate

(a)

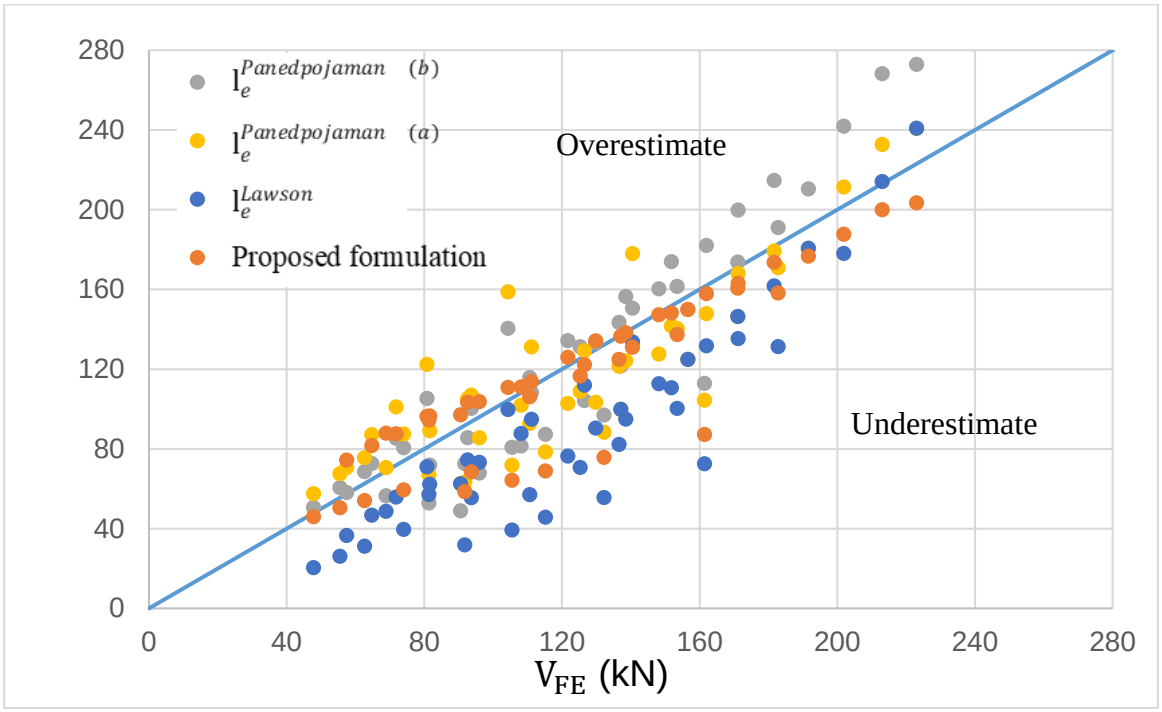
280
240
200
160
120
80
40
0
0
40
80
120
160
200
240
280
V_{FE} (kN)
$l_e^{Panedpojaman\ (b)}$
$l_e^{Panedpojaman\ (a)}$
l_e^{Lawson}
Proposed formulation
Overestimate
Underestimate

(b)

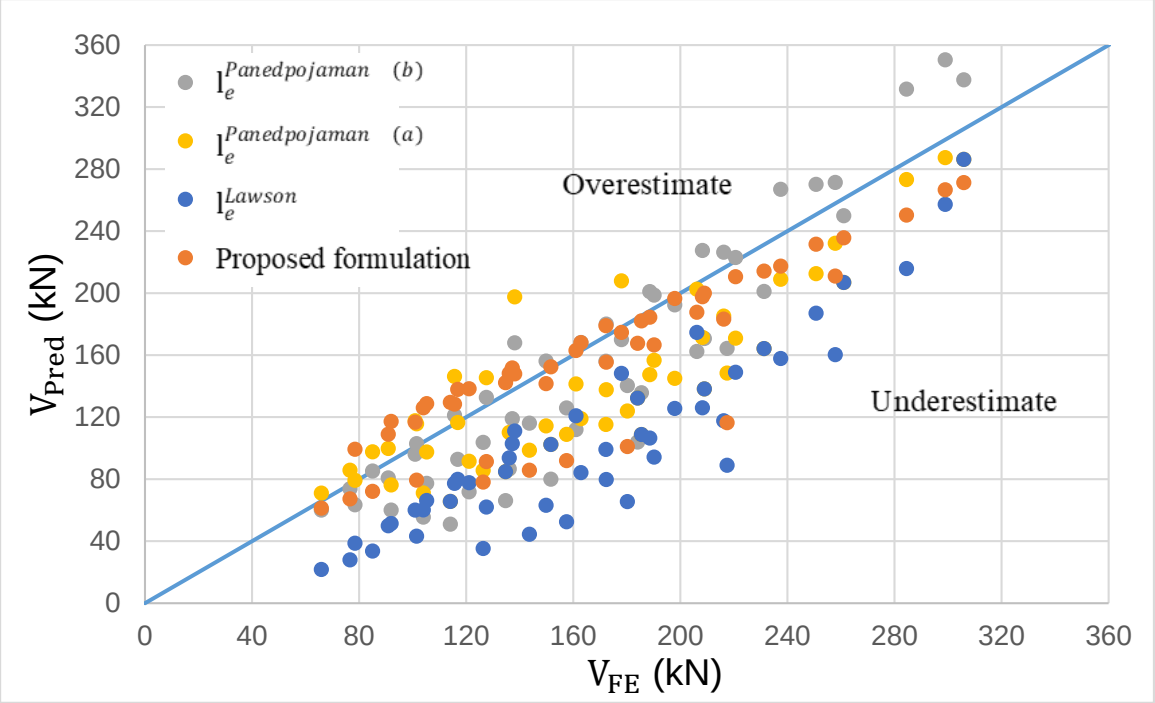

(c)

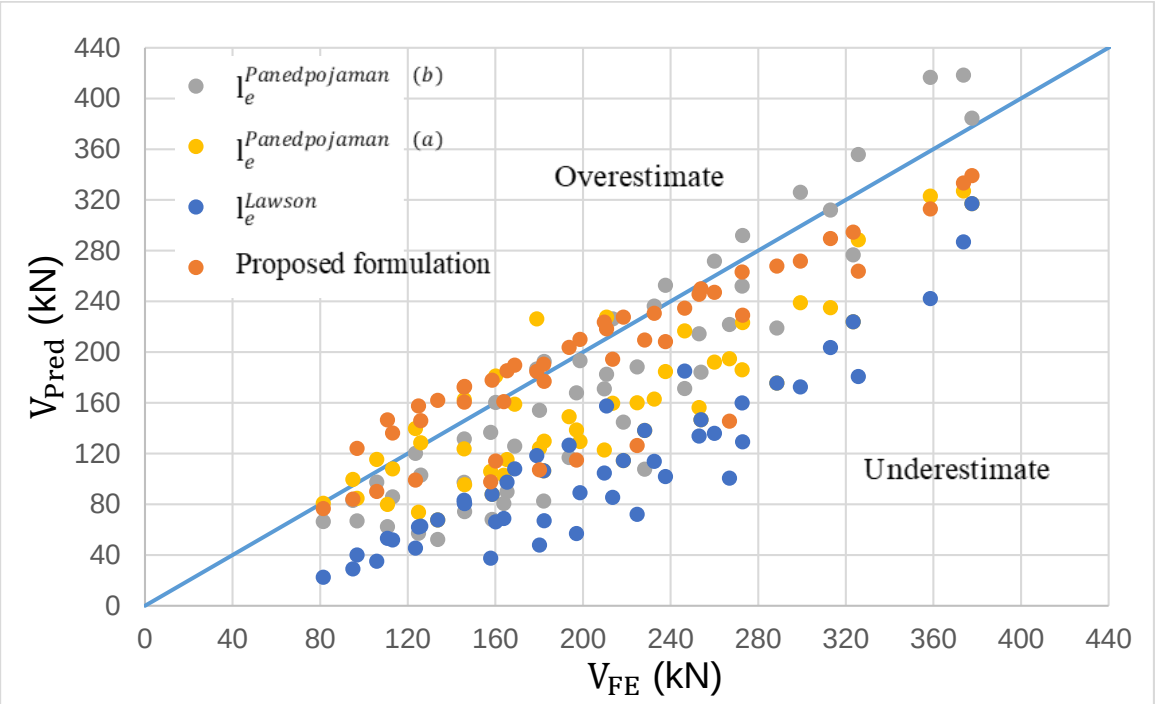

(d)

Figure 21: Comparison of the predicted shear strength with the FE shear strength for beams made from (a) S355; (b) S460; (c) S690; and (d) S960 steel grades

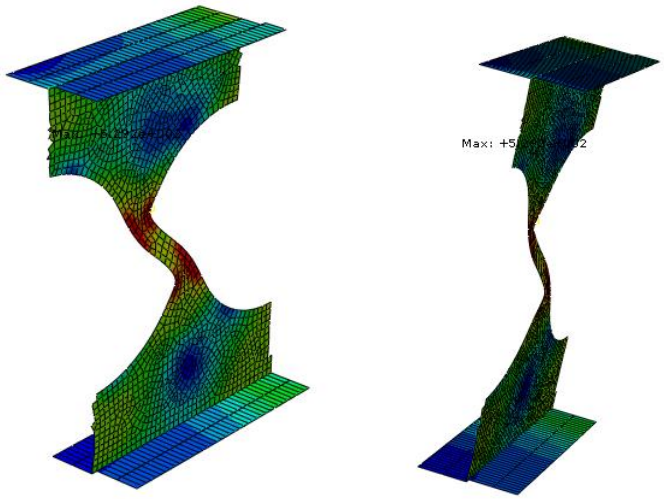

Figure 22: Failure modes different from web-post buckling.

Table 1: Comparison between experimental and numerical buckling shear load

Specimen	Buckling shear load, V (kN)		
	Test V_{test}	Numerical V_{FE}	V_{test}/V_{FE} %
A1	38.0	40.0	5.3
A2	61.9	59.2	-4.3
A3	70.7	65.6	-7.2
A5	99.1	98.4	-0.7
A6	102.2	102.5	0.3
B1	54	54.9	1.6
B2	79	75.6	-4.3
B5	138.5	134.5	-2.9
B6	150	148.6	-0.9
C1	144.4	147.7	2.3
C2	127.5	120	-5.9

Table 2: Material properties of cellular beams for the parametric study [20]

Steel Grade	f_y (MPa)	f_u (MPa)	ε_{st} (%)	ε_u (%)
S355	355	510	2.5	18
S460	460	550	2.0	14
S690	690	770	ε_y	8.8
S960	960	980	ε_y	5.5

Table 3: Ratio of the predicted shear strength to FE shear strength V/V_{FE} based on the effective length model l_e^{Lawson}, $l_e^{Panedpojaman(a)}$ and $l_e^{Panedpojaman(b)}$ and new proposal for S355 steel grade

s/d_o	H/d_o	V/V_{FE}	d/t_w				
			59.8	**54.46**	**50.83**	**46.21**	**40.13**
1.1	**1.25**	$l_e^{Panedpojaman(b)}$	1.07	1.08	1.07	1.06	1.03
		$l_e^{Panedpojaman(a)}$	1.18	1.17	1.16	1.13	1.08
		l_e^{Lawson}	0.47	0.51	0.54	0.58	0.63
		proposed formulation	0.93	0.87	0.83	0.78	0.72
	1.67	$l_e^{Panedpojaman(b)}$	0.73	0.70	0.67	0.64	0.62
		$l_e^{Panedpojaman(a)}$	0.65	0.64	0.62	0.59	0.58
		l_e^{Lawson}	0.37	0.39	0.40	0.41	0.43
		proposed formulation	0.62	0.59	0.56	0.53	0.51
1.2	**1.25**	$l_e^{Panedpojaman(b)}$	1.14	1.24	1.28	1.35	1.44
		$l_e^{Panedpojaman(a)}$	1.35	1.45	1.48	1.53	1.59
		l_e^{Lawson}	0.74	0.82	0.88	0.95	1.08
		proposed formulation	1.31	1.27	1.22	1.16	1.09
	1.67	$l_e^{Panedpojaman(b)}$	1.03	1.02	1.02	1.00	0.98
		$l_e^{Panedpojaman(a)}$	0.87	0.88	0.89	0.89	0.90
		l_e^{Lawson}	0.57	0.62	0.65	0.68	0.73
		proposed formulation	0.97	0.94	0.92	0.89	0.86
1.3	**1.25**	$l_e^{Panedpojaman(b)}$	0.90	0.96	1.00	1.05	1.18
		$l_e^{Panedpojaman(a)}$	1.11	1.16	1.21	1.25	1.36
		l_e^{Lawson}	0.78	0.83	0.88	0.93	1.06
		proposed formulation	1.23	1.13	1.08	1.00	0.95
	1.67	$l_e^{Panedpojaman(b)}$	1.12	1.14	1.15	1.16	1.18
		$l_e^{Panedpojaman(a)}$	0.90	0.95	0.98	1.01	1.06
		l_e^{Lawson}	0.70	0.75	0.80	0.85	0.92
		proposed formulation	1.04	1.01	0.99	0.97	0.94
1.4	**1.25**	$l_e^{Panedpojaman(b)}$	0.72	0.78	0.83	0.93	0.93*
		$l_e^{Panedpojaman(a)}$	0.91	0.97	1.03	1.13	0.93*
		l_e^{Lawson}	0.78	0.84	0.90	0.99	0.93*
		proposed formulation	1.12	1.04	1.00	0.96	0.93*
	1.67	$l_e^{Panedpojaman(b)}$	1.09	1.13	1.17	1.21	1.26

		$l_e^{Panedpojaman\,(a)}$	0.87	0.94	0.99	1.05	1.13
		l_e^{Lawson}	0.77	0.84	0.89	0.96	1.05
		proposed formulation	1.04	1.01	0.99	0.97	0.95
1.5	**1.25**	$l_e^{Panedpojaman\,(b)}$	0.62	0.69	0.96*	0.92*	0.94*
		$l_e^{Panedpojaman\,(a)}$	0.78	0.87	0.96*	0.92*	0.94*
		l_e^{Lawson}	0.78	0.87	0.96*	0.92*	0.94*
		proposed formulation	1.06	1.01	0.96*	0.92*	0.94*
	1.67	$l_e^{Panedpojaman\,(b)}$	0.97	1.04	1.10	1.16	1.26
		$l_e^{Panedpojaman\,(a)}$	0.81	0.89	0.95	1.02	1.14
		l_e^{Lawson}	0.81	0.89	0.95	1.02	1.14
		proposed formulation	0.99	0.97	0.96	0.93	0.92

* Failure by Vierendeel mechanism.

Table 4: Ratio of the predicted shear sterngth to FE shear strength V/V_{FE} based on the effective length model l_e^{Lawson}, $l_e^{Panedpojaman\,(a)}$ and $l_e^{Panedpojaman\,(b)}$ and new proposal for S460 steel grade

s/d_o	H/d_o	V/V_{FE}	d/t_w				
			59.8	**54.46**	**50.83**	**46.21**	**40.13**
1.1	**1.25**	$l_e^{Panedpojaman\,(b)}$	1.06	1.09	1.09	1.09	1.07
		$l_e^{Panedpojaman\,(a)}$	1.20	1.22	1.21	1.18	1.14
		l_e^{Lawson}	0.43	0.47	0.50	0.53	0.59
		proposed formulation	0.96	0.91	0.86	0.80	0.73
	1.67	$l_e^{Panedpojaman\,(b)}$	0.79	0.77	0.76	0.73	0.70
		$l_e^{Panedpojaman\,(a)}$	0.69	0.68	0.68	0.67	0.65
		l_e^{Lawson}	0.35	0.37	0.40	0.42	0.45
		proposed formulation	0.64	0.61	0.60	0.57	0.54
1.2	**1.25**	$l_e^{Panedpojaman\,(b)}$	1.01	1.12	1.19	1.30	1.35
		$l_e^{Panedpojaman\,(a)}$	1.23	1.34	1.41	1.51	1.52
		l_e^{Lawson}	0.64	0.72	0.78	0.88	0.96
		proposed formulation	1.29	1.26	1.22	1.19	1.06
	1.67	$l_e^{Panedpojaman\,(b)}$	1.05	1.05	1.05	1.05	1.04
		$l_e^{Panedpojaman\,(a)}$	0.84	0.87	0.89	0.91	0.93
		l_e^{Lawson}	0.52	0.56	0.60	0.65	0.72
		proposed formulation	0.96	0.93	0.91	0.89	0.86
1.3	**1.25**	$l_e^{Panedpojaman\,(b)}$	0.82	0.88	0.92	0.97	1.07
		$l_e^{Panedpojaman\,(a)}$	1.02	1.09	1.14	1.18	1.27
		l_e^{Lawson}	0.71	0.76	0.80	0.85	0.95
		proposed formulation	1.28	1.18	1.12	1.02	0.93
	1.67	$l_e^{Panedpojaman\,(b)}$	1.10	1.13	1.15	1.17	1.20
		$l_e^{Panedpojaman\,(a)}$	0.84	0.90	0.93	0.98	1.05
		l_e^{Lawson}	0.63	0.68	0.73	0.79	0.88
		proposed formulation	1.03	1.00	0.98	0.95	0.93
1.4	**1.25**	$l_e^{Panedpojaman\,(b)}$	0.65	0.71	0.75	0.82	1.00*
		$l_e^{Panedpojaman\,(a)}$	0.82	0.89	0.94	1.02	1.00*
		l_e^{Lawson}	0.70	0.76	0.81	0.88	1.00*
		proposed formulation	1.16	1.08	1.03	0.97	1.00*
	1.67	$l_e^{Panedpojaman\,(b)}$	1.03	1.08	1.12	1.18	1.26

		$l_e^{Panedpojaman\,(a)}$	0.80	0.86	0.91	0.99	1.09
		l_e^{Lawson}	0.70	0.76	0.81	0.89	1.00
		proposed formulation	1.03	0.99	0.97	0.96	0.94
1.5	**1.25**	$l_e^{Panedpojaman\,(b)}$	0.54	0.60	0.65	1.00*	1.02*
		$l_e^{Panedpojaman\,(a)}$	0.69	0.76	0.83	1.00*	1.02*
		l_e^{Lawson}	0.69	0.76	0.83	1.00*	1.02*
		proposed formulation	1.07	1.01	0.98	1.00*	1.02*
	1.67	$l_e^{Panedpojaman\,(b)}$	0.89	0.96	1.01	1.10	1.22
		$l_e^{Panedpojaman\,(a)}$	0.73	0.80	0.86	0.94	1.08
		l_e^{Lawson}	0.73	0.80	0.86	0.94	1.08
		proposed formulation	1.00	0.96	0.94	0.92	0.91

* Failure by Vierendeel mechanism.

Table 5: Ratio of the predicted shear sterngth to FE shear strength V/V_{FE} based on the effective length model l_e^{Lawson}, $l_e^{Panedpojaman\,(a)}$ and $l_e^{Panedpojaman\,(b)}$ and new proposal for S690 steel grade

s/d_o	H/d_o	V/V_{FE}	d/t_w				
			59.8	**54.46**	**50.83**	**46.21**	**40.13**
1.1	**1.25**	$l_e^{Panedpojaman\,(b)}$	0.91	0.96	1.00	1.01	1.04
		$l_e^{Panedpojaman\,(a)}$	1.08	1.12	1.15	1.14	1.14
		l_e^{Lawson}	0.33	0.36	0.39	0.42	0.49
		proposed formulation	0.93	0.88	0.85	0.78	0.71
	1.67	$l_e^{Panedpojaman\,(b)}$	0.82	0.81	0.80	0.78	0.76
		$l_e^{Panedpojaman\,(a)}$	0.68	0.69	0.69	0.69	0.68
		l_e^{Lawson}	0.28	0.31	0.33	0.36	0.41
		proposed formulation	0.62	0.60	0.58	0.56	0.53
1.2	**1.25**	$l_e^{Panedpojaman\,(b)}$	0.81	0.89	0.95	1.05	1.21
		$l_e^{Panedpojaman\,(a)}$	1.01	1.10	1.16	1.26	1.43
		l_e^{Lawson}	0.49	0.55	0.59	0.67	0.80
		proposed formulation	1.26	1.20	1.16	1.11	1.07
	1.67	$l_e^{Panedpojaman\,(b)}$	1.04	1.04	1.04	1.05	1.05
		$l_e^{Panedpojaman\,(a)}$	0.76	0.80	0.82	0.86	0.90
		l_e^{Lawson}	0.42	0.46	0.49	0.54	0.62
		proposed formulation	0.94	0.90	0.88	0.85	0.82
1.3	**1.25**	$l_e^{Panedpojaman\,(b)}$	0.65	0.73	0.79	0.87	0.95
		$l_e^{Panedpojaman\,(a)}$	0.83	0.93	1.00	1.08	1.17
		l_e^{Lawson}	0.56	0.63	0.68	0.75	0.83
		proposed formulation	1.27	1.22	1.18	1.10	0.98
	1.67	$l_e^{Panedpojaman\,(b)}$	1.03	1.07	1.09	1.12	1.16
		$l_e^{Panedpojaman\,(a)}$	0.73	0.78	0.82	0.88	0.96
		l_e^{Lawson}	0.52	0.56	0.60	0.66	0.76
		proposed formulation	1.03	0.98	0.95	0.91	0.88
1.4	**1.25**	$l_e^{Panedpojaman\,(b)}$	0.53	0.59	0.64	0.69	0.79
		$l_e^{Panedpojaman\,(a)}$	0.68	0.76	0.81	0.88	0.98
		l_e^{Lawson}	0.58	0.64	0.69	0.75	0.85
		proposed formulation	1.21	1.14	1.09	1.01	0.91
	1.67	$l_e^{Panedpojaman\,(b)}$	0.91	0.97	1.01	1.08	1.17

		$l_e^{Panedpojaman\,(a)}$	0.67	0.73	0.77	0.85	0.96
		l_e^{Lawson}	0.58	0.63	0.67	0.75	0.86
		proposed formulation	1.04	0.99	0.95	0.92	0.89
1.5	**1.25**	$l_e^{Panedpojaman\,(b)}$	0.45	0.49	0.53	0.56	1.02*
		$l_e^{Panedpojaman\,(a)}$	0.57	0.63	0.67	0.72	1.02*
		l_e^{Lawson}	0.57	0.63	0.67	0.72	1.02*
		proposed formulation	1.13	1.05	1.00	0.91	1.02*
	1.67	$l_e^{Panedpojaman\,(b)}$	0.73	0.82	0.87	0.96	1.10
		$l_e^{Panedpojaman\,(a)}$	0.59	0.66	0.71	0.79	0.94
		l_e^{Lawson}	0.59	0.66	0.71	0.79	0.94
		proposed formulation	0.98	0.96	0.93	0.90	0.89

* Failure by Vierendeel mechanism.

Table 6: Ratio of the predicted shear sterngth to FE shear strength V/V_{FE} based on the effective length model l_e^{Lawson}, $l_e^{Panedpojaman\,(a)}$ and $l_e^{Panedpojaman\,(b)}$ and new proposal for S960 steel grade

s/d_o	H/d_o	V/V_{FE}	d/t_w				
			59.8	**54.46**	**50.83**	**46.21**	**40.13**
1.1	**1.25**	$l_e^{Panedpojaman\,(b)}$	0.81	0.87	0.92	0.97	1.00
		$l_e^{Panedpojaman\,(a)}$	0.99	1.05	1.09	1.13	1.13
		l_e^{Lawson}	0.27	0.31	0.33	0.37	0.41
		proposed formulation	0.94	0.88	0.85	0.80	0.71
	1.67	$l_e^{Panedpojaman\,(b)}$	0.86	0.85	0.85	0.84	0.83
		$l_e^{Panedpojaman\,(a)}$	0.67	0.69	0.70	0.71	0.73
		l_e^{Lawson}	0.24	0.26	0.29	0.32	0.38
		proposed formulation	0.62	0.59	0.58	0.56	0.54
1.2	**1.25**	$l_e^{Panedpojaman\,(b)}$	0.69	0.76	0.82	0.90	1.04
		$l_e^{Panedpojaman\,(a)}$	0.87	0.95	1.02	1.11	1.26
		l_e^{Lawson}	0.41	0.46	0.50	0.56	0.66
		proposed formulation	1.28	1.20	1.16	1.10	1.03
	1.67	$l_e^{Panedpojaman\,(b)}$	1.06	1.06	1.06	1.07	1.09
		$l_e^{Panedpojaman\,(a)}$	0.71	0.75	0.78	0.82	0.89
		l_e^{Lawson}	0.37	0.40	0.43	0.47	0.55
		proposed formulation	0.97	0.91	0.88	0.84	0.81
1.3	**1.25**	$l_e^{Panedpojaman\,(b)}$	0.56	0.49	0.67	0.74	0.86
		$l_e^{Panedpojaman\,(a)}$	0.72	0.63	0.85	0.94	1.08
		l_e^{Lawson}	0.48	0.42	0.57	0.64	0.75
		proposed formulation	1.32	0.98	1.18	1.12	1.04
	1.67	$l_e^{Panedpojaman\,(b)}$	0.97	1.01	1.04	1.09	1.16
		$l_e^{Panedpojaman\,(a)}$	0.65	0.70	0.74	0.80	0.90
		l_e^{Lawson}	0.45	0.49	0.52	0.58	0.67
		proposed formulation	1.06	0.99	0.95	0.91	0.87
1.4	**1.25**	$l_e^{Panedpojaman\,(b)}$	0.46	0.51	0.54	0.60	0.69
		$l_e^{Panedpojaman\,(a)}$	0.59	0.65	0.70	0.77	0.88
		l_e^{Lawson}	0.50	0.55	0.59	0.65	0.75
		proposed formulation	1.26	1.18	1.12	1.05	0.95
	1.67	$l_e^{Panedpojaman\,(b)}$	0.81	0.85	0.92	1.00	1.12

		$l_e^{Panedpojaman\,(a)}$	0.58	0.62	0.68	0.75	0.87
		l_e^{Lawson}	0.50	0.53	0.59	0.65	0.77
		proposed formulation	1.07	0.97	0.96	0.92	0.89
1.5	**1.25**	$l_e^{Panedpojaman\,(b)}$	0.39	0.43	0.45	0.47	0.57
		$l_e^{Panedpojaman\,(a)}$	0.51	0.55	0.58	0.61	0.73
		l_e^{Lawson}	0.51	0.55	0.58	0.61	0.73
		proposed formulation	1.21	1.12	1.05	0.92	0.87
	1.67	$l_e^{Panedpojaman\,(b)}$	0.66	0.72	0.76	0.85	1.02
		$l_e^{Panedpojaman\,(a)}$	0.52	0.58	0.61	0.69	0.84
		l_e^{Lawson}	0.52	0.58	0.61	0.69	0.84
		proposed formulation	1.04	0.98	0.93	0.91	0.90

Table 7: Summary of RMS errors

Steel Grade	Analytical model	RMS error
S355	$l_e^{Panedpojaman\,(b)}$	21.8
	$l_e^{Panedpojaman\,(a)}$	21.8
	l_e^{Lawson}	29.3
	proposed formulation	18.5
S460	$l_e^{Panedpojaman\,(b)}$	25.1
	$l_e^{Panedpojaman\,(a)}$	24.5
	l_e^{Lawson}	38.3
	proposed formulation	22.5
S690	$l_e^{Panedpojaman\,(b)}$	33.9
	$l_e^{Panedpojaman\,(a)}$	38.9
	l_e^{Lawson}	67.3
	proposed formulation	29.8
S960	$l_e^{Panedpojaman\,(b)}$	49.1
	$l_e^{Panedpojaman\,(a)}$	59.7
	l_e^{Lawson}	99.5
	proposed formulation	37.1

Table 8: Summary of the reliability analysis for the proposed formulation (s/do=1.1 cases included).

	n	$\bar{b}$	$k_{d,n}$	V_r	γ_{M0}
S355	46	1.05	3.04	0.23	1.44
S460	45	1.11	3.04	0.22	1.55
S690	49	1.07	3.04	0.22	1.55
S960	49	1.09	3.04	0.22	1.56

Table 9: Summary of the reliability analysis for the proposed formulation (s/do=1.1 cases excluded).

	n	$\bar{b}$	$k_{d,n}$	V_r	γ_{M0}
S355	41	1.02	3.04	0.137	1.16
S460	40	1.03	3.04	0.14	1.29
S690	44	1.05	3.04	0.15	1.31
S960	44	1.04	3.04	0.152	1.32